Global Biogeochemical Cycles®

RESEARCH ARTICLE
10.1029/2021GB007187

Benthic Organic Matter Transformation Drives pH and Carbonate Chemistry in Arctic Marine Sediments

F. S. Freitas[1,2], S. Arndt[2], K. R. Hendry[1,3], J. C. Faust[4], A. C. Tessin[5], and C. März[6,7]

[1]School of Earth Sciences, University of Bristol, Bristol, UK, [2]BGeosys, Department of Earth and Environmental Sciences, Université Libre de Bruxelles, Brussels, Belgium, [3]British Antarctic Survey, Cambridge, UK, [4]MARUM-Center for Marine Environmental Sciences, University of Bremen, Bremen, Germany, [5]Department of Geology, Kent State University, Kent, OH, USA, [6]School of Earth & Environment, University of Leeds, Leeds, UK, [7]Institut für Geowissenschaften, Universität Bonn, Bonn, Germany

Abstract Carbonate chemistry of the Arctic Ocean seafloor and its vulnerability to ocean acidification remains poorly explored. This limits our ability to quantify how biogeochemical processes and bottom water conditions shape sedimentary carbonate chemistry, and to predict how climate change may affect such biogeochemical processes at the Arctic Ocean seafloor. Here, we employ an integrated data-model assessment that explicitly resolves benthic pH and carbonate chemistry along a South—North transect in the Barents Sea. We identify the main drivers of observed carbonate dynamics and estimate benthic fluxes of dissolved inorganic carbon and alkalinity to the Arctic Ocean. We explore how bottom water conditions and in-situ organic matter degradation shape these processes and show that organic matter transformation strongly impacts pH and carbonate saturation (Ω) variations. Aerobic organic matter degradation drives a negative pH shift (pH < 7.6) in the upper 2–5 cm, producing Ω < 1. This causes shallow carbonate dissolution, buffering porewater pH to around 8.0. Organic matter degradation via metal oxide (Mn/Fe) reduction pathways further increases pH and carbonate saturation state. At the northern stations, where Ω > 5 at around 10–25 cm, model simulations result in authigenic carbonate precipitation. Furthermore, benthic fluxes of dissolved inorganic carbon (12.5–59.5 μmol cm^{-2} yr^{-1}) and alkalinity (11.3–63.2 μmol cm^{-2} yr^{-1}) are 2–3-fold greater in the northern sites due to greater carbonate dissolution. Our assessment is of significant relevance to predict how changes in the Arctic Ocean may shift carbon burial and pH buffering into the next century.

Plain Language Summary The Arctic Ocean seafloor is an important place for long-term storage of carbon, locking it away from the atmosphere. However, such storage capacity is also vulnerable itself to climate change. Thus, we need to understand how carbon is recycled and packed away in the Arctic seafloor to be able to predict future shifts in Earth's climate. We use the Barents Sea to study carbon recycling in the seafloor and to make predictions of possible impacts of climate change. We use a model that computes chemical processes at the seafloor. This allows us to investigate how organic carbon recycling at the seafloor, and saturation state of bottom waters, can impact the dissolution of inorganic carbon, which then leads to the release of carbon back to Arctic Ocean waters. We also test how possible environmental conditions arising from climate change could impact carbon storage in the Arctic Ocean seafloor. We find important climate feedbacks, for example, that further acidification of bottom waters could reduce inorganic carbon storage, whereas greater deposition and recycling of organic carbon could help locking inorganic carbon within seafloor. These results can help scientists and policy makers finding ways of mitigating the effects of climate change in the future.

F. S. Freitas and S. Arndt contributed equally to this work.

Key Points:

- Changes in pH and carbonate saturation state of Barents Sea sediments are driven by organic matter degradation and bottom water chemistry
- Metabolic dissolution of $CaCO_3$ in the top 5 cm depth buffers pH and saturation state, enabling carbonate precipitation in deeper sediments
- Higher benthic fluxes of alkalinity and dissolution of inorganic carbon from South to North reflect greater carbonate dissolution in the northern Barents Sea sites

Supporting Information:

Supporting Information may be found in the online version of this article.

Correspondence to:

F. S. Freitas,
felipe.salesdefreitas@bristol.ac.uk

Citation:

Freitas, F. S., Arndt, S., Hendry, K. R., Faust, J. C., Tessin, A. C., & März, C. (2022). Benthic organic matter transformation drives pH and carbonate chemistry in Arctic marine sediments. *Global Biogeochemical Cycles*, *36*, e2021GB007187. https://doi.org/10.1029/2021GB007187

Received 10 SEP 2021
Accepted 12 JUN 2022

Author Contributions:

Conceptualization: F. S. Freitas, S. Arndt
Formal analysis: F. S. Freitas
Funding acquisition: S. Arndt, K. R. Hendry, C. März
Methodology: F. S. Freitas, S. Arndt
Project Administration: K. R. Hendry, C. März
Software: F. S. Freitas, S. Arndt

1. Introduction

The Arctic Ocean, and in particular its seasonally ice-free areas, is highly vulnerable to ocean acidification (OA) due to its large carbon dioxide (CO_2) uptake capacity. It acts as a global hotspot of atmospheric CO_2 drawdown due to its permanently cold surface waters, its undersaturation with respect to CO_2, and brine rejection during sea-ice formation that mixes surface CO_2 into deeper water layers (Chen & Borges, 2009; Kaltin et al., 2002). Air-sea CO_2 exchange exerts an important control on seawater pH and its carbonate saturation state (Ω) (Millero, 2000; Zeebe & Wolf-Gladrow, 2001). An increase in atmospheric CO_2 level (e.g., by anthropogenic emissions) can induce negative shifts in pH and Ω (Bindoff et al., 2019; Friedlingstein et al., 2019), leading to OA (Doney et al., 2020; Gattuso & Hansson, 2011). In addition to air-sea CO_2 fluxes, the carbonate chemistry of the Arctic Ocean is further modulated by the distribution of water masses with contrasting physico-chemical

Validation: F. S. Freitas
Visualization: F. S. Freitas
Writing – original draft: F. S. Freitas, S. Arndt
Writing – review & editing: K. R. Hendry, J. C. Faust, A. C. Tessin, C. März

characteristics, the seasonal sea-ice dynamics, and fluctuations of riverine discharge, permafrost thawing, coastal erosion, and gas hydrate destabilization (Bates & Mathis, 2009; Cai et al., 2010; Else et al., 2013; Middelburg et al., 2020; Semiletov et al., 2016). These processes can contribute to pH and Ω shifts in shallow and deeper water masses, which can become undersaturated with respect to particulate inorganic carbon (PIC) phases, that is, carbonate minerals (aragonite and calcite) (Millero, 2000; Zeebe & Wolf-Gladrow, 2001). Such saturation changes can negatively impact Arctic ecosystems, in particular carbonate-shelled organisms (Fabry et al., 2008; Guinotte & Fabry, 2008; Kroeker et al., 2010), reduce PIC export to the seafloor (Luo et al., 2016; Y. Zhang et al., 2020), and affect long-term inorganic carbon burial, and redox processes in Arctic Ocean sediments (Gazeau et al., 2014). Currently, across most of the Arctic Ocean the calcite compensation depth is situated at around 4,000 m water depth, whereas aragonite displays a much shallower compensation depth at 2,000 m (Jutterström & Anderson, 2005). However, undersaturation of shallower waters with respect to aragonite is already documented in the Beaufort Gyre (Y. Zhang et al., 2020) and across the East Siberian Shelf (Semiletov et al., 2016). Model results further predict an overall shoaling of both aragonite and calcite compensation depths in the Arctic Ocean due to enhanced CO_2 emissions in the next hundred years (Luo et al., 2016).

Changes in the carbonate chemistry of the Arctic Ocean not only impact the pelagic system. Crucially, and somewhat underexplored in the Arctic, they also exert an influence on the seafloor. Given the low bottom water pH values found in the Arctic Ocean (Jones et al., 2019; Kostka et al., 1999), a decrease in PIC fluxes would suppress the buffering capacity of the sediment, with implications for pH and Ω at the sediment-water interface (SWI) (Middelburg, 2019). Field and laboratory studies show that acidification of the Arctic Ocean can induce a decrease in sedimentary porewater pH, as well as a further decrease in carbonate deposition with important implications for porewater Ω, and thus changes in dissolved inorganic carbon (DIC) and total alkalinity (TA) dynamics (Gazeau et al., 2014; Jutterström & Anderson, 2005). Consequently, Arctic marine sediments can experience a decrease of pH buffering capacity in response to OA (Bates & Mathis, 2009). Yet, benthic inorganic carbon dynamics and porewater pH and saturation state are not only controlled by bottom water carbonate saturation and PIC deposition. They are also influenced by the complex and dynamic diagenetic processes within the sediment. These sub-seafloor processes control sediment-water exchange fluxes and burial fluxes, and thus exert a feedback on ocean carbonate chemistry (Krumins et al., 2013; Morse & Mackenzie, 1990; Soetaert et al., 2007).

In marine sediments, there is hardly a biogeochemical process that does not affect the depth evolution of porewater pH through the production or consumption of protolytic species of the carbonate and sulfide systems (Blouet et al., 2021; Jourabchi et al., 2005; Morse & Mackenzie, 1990). However, the influence of each biogeochemical reaction on porewater pH is not only dependent on the production/consumption rates of these protolytic species, but is also controlled by the ambient pH itself (Jourabchi et al., 2005; Soetaert et al., 2007). In marine sediments within a pH range of 6.5–8.5, some key biogeochemical processes involving organic matter (OM) transformation can be summarized as follows (Figure 1). (a) Aerobic reactions (OM degradation coupled to oxygen consumption and reoxidation of reduced species—e.g., ammonium, dissolved manganese, dissolved iron, and hydrogen sulfide – coupled to oxygen) generally produce negative shifts in porewater pH (Cai et al., 2000; Cai & Reimers, 1993; Canfield et al., 1993; Forja et al., 2004; Jourabchi et al., 2005; Mucci et al., 2000; Soetaert et al., 2007). Consequently, these processes are generally considered the main drivers of carbonate dissolution that occurs in the upper, well-mixed sediment layers (Adler et al., 2001; Berelson et al., 1990; 1994; Emerson & Archer, 1990; Hales et al., 1994; Jahnke et al., 1994; 1997; Jahnke & Jahnke, 2000; 2004). (b) OM oxidation coupled to manganese (Mn) and iron (Fe) (oxyhydr)oxide reduction consumes protolytic species, thus increases the ambient pH (Kostka et al., 1999; Krumins et al., 2013; Soetaert et al., 2007; Tessin et al., 2020). These processes result in TA production and can drive carbonate oversaturation in porewaters (e.g., Berner et al., 1970; Hu & Cai, 2011), which can favor benthic foraminiferal biomineralization (Green & Aller, 2001). In contrast to metal oxide metabolic pathways, the influence of organoclastic sulfate reduction (OSR) on porewater pH and Ω is more sensitive to ambient pH conditions because the concomitant production of alkalinity, as well as total dissolved sulfides which can result in either proton production or consumption (Ben-Yaakov, 1973; Blouet et al., 2021; Jourabchi et al., 2005; Mackenzie et al., 1995; Soetaert et al., 2007). In general, OSR consumes protolytic species at ambient pH $\leq$ 6.9, but switches to protolytic species production at pH > 6.9 (Blouet et al., 2021; Soetaert et al., 2007). At a typical porewater pH, total dissolved sulfide hence dissociates into H_2S and releases protons, thus outcompeting the carbonate alkalinity. However, if OSR is quantitatively coupled to the precipitation and burial of iron sulfide minerals that remove total dissolved sulfides, OSR will result in a pH increase and carbonate oversaturation of porewaters (e.g., Ben-Yaakov, 1973; Rassmann et al., 2020).

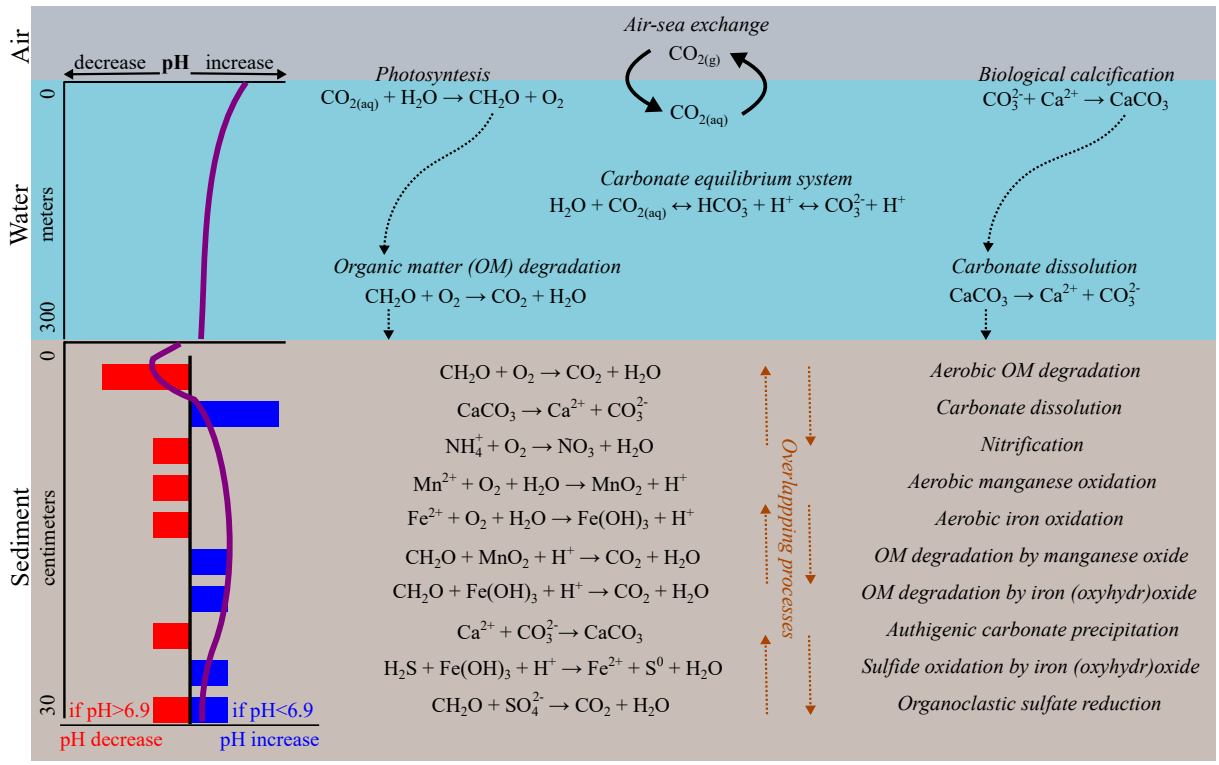

Figure 1. Simplified overview of processes driving carbonate chemistry in marine systems from air (gray box) to water (cyan box) and seafloor (brown box). Reactions are not stoichiometrically balanced and only display key species. For complete reaction network see Table S1. The purple lines illustrate changes in pH profiles as a result of biogeochemical processes. The red bars indicate negative shifts in pH, whereas the blue bars denote positive changes in pH by reactions. Size of bars is not quantitative. Changes in pH are assumed for a typical ambient pH interval of 6.5–8.5. Changes in pH due to organoclastic sulfate reduction can be either positive or negative for the assumed ambient pH interval (see text). Dashed brown arrows indicate that some biogeochemical processes can overlap within sediments. Depicted processes are adapted from Millero (2000) and Soetaert et al. (2007).

Overall, the processes described above show how complex and dynamic the interplay of OM degradation and reoxidation processes are at the seafloor and emphasizes the challenges of fully capturing the controls of pH and carbonate chemistry in Arctic sediments. Therefore, systematically understanding which diagenetic processes governs pH and Ω changes is not only fundamental for constraining the present-day carbonate system of the Arctic seafloor, but also critical for assessing how these processes could respond to projected changes in environmental conditions. Here, we employ an integrated model-data assessment that explicitly resolves benthic pH and carbonate chemistry in Barents Sea shelf sediments to quantify carbonate dynamics, to identify its main drivers, and to understand DIC and TA fluxes to the Arctic Ocean. We investigate five stations (B13–B17; Table 1; Figure 2) along a 30°E South—North transect (for details, see Faust et al., 2020; 2021; Freitas et al., 2020). We apply a Reaction-Transport Model (RTM) approach (a) to reproduce the downcore evolution of porewater and sediment depths profiles including carbonate system parameters (pH, DIC, TA, and Ω), (b) to quantify the relative

Table 1
Site-Specific Model Parameters Prescribed to Reproduce pH and Carbonate System Downcore Evolution

			Bottom water		Sediment-water interface			
Site	Latitude °N	Depth m	Temperature °C	Salinity	pH	TA µM	$CaCO_3$ wt%	Ca^{2+} mM
B17	81.5	291	1.76	34.9	7.20	2,350	3.29	12.6
B16	80.1	294	−1.44	34.7	7.44	2,350	3.88	12.0
B15	78.2	330	−1.49	34.9	7.65	2,350	1.34	12.0
B14	76.5	290	1.95	35.0	7.47	2,350	0.77	11.8
B13	74.5	355	1.77	35.0	7.60	2,350	1.78	12.6

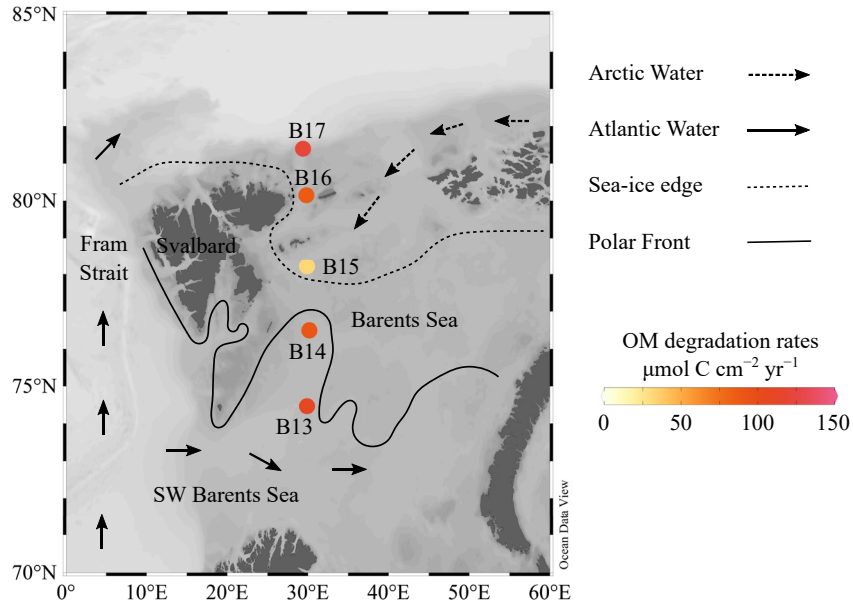

Figure 2. Barents Sea and location of investigated stations (B13–B17) along a 30°E transect. Oceanographic features adapted from Oziel et al. (2016). Organic matter degradation rates are from Freitas et al. (2020). Sea–sea ice edge position in mid-July adapted from the Norwegian Meteorological Institute ice charts (https://cryo.met.no/archive/ice-service/icecharts/quicklooks/2017/). Base map produced with Ocean Data View (Schlitzer, 2021).

contribution of each biogeochemical reaction to porewater pH, carbonate saturation, and carbonate dissolution/precipitation, (c) to quantify benthic effluxes of TA and DIC, and (d) to assess the sensitivity of benthic carbonate dynamics to changing environmental conditions.

2. Methods

2.1. Study Area

The Barents Sea (Figure 2) is the largest shelf area in the Arctic Ocean, located north of Norway and Russia (Carmack & Wassmann, 2006). The prevailing oceanographic conditions are strongly shaped by sea-ice and wind dynamics, as well as bathymetry. These interactions generate the complex boundary between Arctic Water (ArW; low salinity and low nutrients) and Atlantic Water (AW; high salinity and high nutrients), giving rise to the oceanographic Polar Front (PF) (Oziel et al., 2016). Sea-ice extent during spring–summer periods exerts strong influence on pelagic primary productivity and nutrient cycling, resulting in a general S–N zonation (Dalpadado et al., 2020; Downes et al., 2021; Henley et al., 2020; Lewis et al., 2020; Oziel et al., 2020; Reigstad et al., 2008; Tuerena et al., 2021; Wassmann, Slagstad, et al., 2006).

The Barents Sea shelf area is characterized by a strong benthic-pelagic coupling (Wassmann, Reigstad, et al., 2006; Wassmann, Slagstad, et al., 2006). This is manifested through relatively high rates of sediment oxygen demand (≈5–9 mmol m^{-2} d^{-1}; Bourgeois et al., 2017), intense transformation of OM close to the seafloor (Freitas et al., 2020; Nickel et al., 2008; Stevenson et al., 2020; Vandieken et al., 2006), and intricate benthic ecology (Cochrane et al., 2009; Morata & Renaud, 2008; Reigstad et al., 2008; Solan et al., 2020; Souster et al., 2020). We recently applied a model-data approach to quantify benthic OM dynamics along a transect across the Barents Sea shelf (Figure 2; Freitas et al., 2020). Critically, our findings revealed that the overall rates of OM degradation are largely governed by the reactivity of the deposited OM at the seafloor, which is decoupled from the S–N pelagic environmental gradient. Instead, benthic OM reactivity is mainly controlled by the prevailing oceanographic conditions, as well as transport pathways of less reactive OM from terrestrial sources. Lipid biomarker data suggests a dominantly marine character of depositing OM (Stevenson & Abbott, 2019; Stevenson et al., 2020). Yet, comparatively low OM degradation rates and nutrient fluxes are estimated at the central station of our transect (site B15; Figure 2; Freitas et al., 2020). These can be related to the supply of less reactive terrestrial OM

over the central Barents Sea shelf (Martens et al., 2021), which is likely sourced from the Svalbard area (Knies & Stein, 1998; Winkelmann & Knies, 2005; Zaborska et al., 2008).

The pelagic carbonate chemistry of the Barents Sea shelf area is influenced by latitudinal, bathymetric, and sea-ice trends (Jones et al., 2019; Tynan et al., 2016). In the SW Barents Sea (71°N–74°N), surface water pH is lower than on the NE shelf (77°N–80°N) where pH reaches up to 8.23. Generally, pH decreases from surface (pH > 8.10) to deep waters (pH < 8.04) along the shelf. Furthermore, surface water pH changes seasonally, with winter values around 8.05 and summer pH > 8.10 (Jones et al., 2019). The TA in the upper layers (shallower than 200 m) of the SW and S Barents Sea reflects the predominance of warmer and more saline AW, and ranges between 2,310 and 2,330 μM (Jones et al., 2019; Tynan et al., 2016). By contrast, the NE shelf displays the lowest surface (shallower than 50 m) TA values at 80°N, which reflects both sea-ice melting and biological carbon uptake (Jones et al., 2019).

Sedimentary porewater pH at the sediment-water interface (SWI) is generally lower (pH < 7.70) (Husum et al., 2020; Kostka et al., 1999) compared to overlying bottom water (e.g., Jones et al., 2019). Observations of bottom water and porewater TA are rare for the Barents Sea shelf area. A study by Hulth et al. (1996) generally shows TA concentrations of between 2,260 and 2,370 μM at the SWI. However, TA concentrations can deviate locally or temporarily from this generally observed stable pattern. For instance, Hulth et al. (1996) report anomalous low (2,060 μM in June/1991) and high (2,690 μM in July/1991) TA concentrations at the SWI in an area located in the SE shelf. However, it remains unclear if such discrepancy in TA resulted from seasonal and/or site-specific conditions or sampling/analytical artifacts. Carbonate contents within the Barents Sea surface sediments reveal higher values on the SW and Norwegian shelves (>5 wt%), relatively lower contents in the vicinity of the Polar Front (<1.5 wt%), and moderate amounts on the northern shelf (3–5 wt%) (Faust et al., 2020 and references therein). Biogenic calcite is the predominant form of calcium carbonate ($CaCO_3$) across the Barents Sea; dolomite is only present in small amounts and linked to coarse detrital sediment input (Demina et al., 2020; Pautova et al., 2020; Solheim & Elverhoi, 1996).

2.2. Model Approach

We adopt the Biogeochemical Reaction Network Simulator (BRNS), a flexible simulation environment suitable for large, mixed kinetic-equilibrium reaction networks (Aguilera et al., 2005; Regnier et al., 2002). We extend the set-up of the BRNS for the Barents Sea sites that was recently applied for investigating and quantifying seafloor OM transformation dynamics (Freitas et al., 2020) by explicitly including pH and carbonate dynamics (Section 2.2.1) and forcing the model with site-specific SWI conditions for these new variables (Table 1). A detailed description of the OM model, its assumptions, and parametrizations can be found in Freitas et al. (2020; 2021). A brief model description and parametrization of OM dynamics is presented in the supplements (Supporting Information S1). Importantly, we do not fit the model to carbonate parameters (pH, DIC, $CaCO_3$, and Ca^{2+}). Instead, we use the model set-up that has previously been calibrated on the basis of observed OM, terminal electron acceptor, and nutrient profiles, as well as its underlying assumptions (Supporting Information S1; Freitas et al., 2020) to predict seafloor carbonate dynamics driven by benthic biogeochemical dynamics. The generally good agreement with observed carbonate dynamics (Section 3.1) offers independent validation for the previously simulated OM dynamics (Freitas et al., 2020) and allows us to disentangle and quantify the influence of different diagenetic processes on pH and carbonate systems in the Barents Sea sediments. Here, we provide a brief description of the newly implemented pH and carbonate system framework, which explicitly resolves downcore evolutions of pH, DIC, and TA. For an overview of the reaction network, see Table S1.

2.2.1. pH and Carbonate System

Porewater pH (Equation 1), DIC (Equation 2), and TA (Equation 3) are defined as (Millero, 2000; Zeebe & Wolf-Gladrow, 2001):

$$pH = -\log_{10} H^+ \tag{1}$$

$$DIC = CO_2 + HCO_3^- + CO_3^{2-} \tag{2}$$

$$TA = HCO_3^- + 2 \cdot CO_3^{2-} + B(OH)_4^- + HS^- \tag{3}$$

The species accounted in Equation 3 represent the major contributions to porewater TA in porewaters, whereas protons and hydroxyl ions are assumed to be negligible (Jourabchi et al., 2005). Furthermore, bicarbonate (HCO_3^-), carbonate (CO_3^{2-}), and borate ($B(OH)_4^-$) ions account for greater than 99% of TA (e.g., Zeebe & Wolf-Gladrow, 2001).

We assume that calcite is the predominant form of $CaCO_3$ deposited in the Barents Sea sediments (Section 2.1). Therefore, we utilize the apparent dissociation constant (K'_{sp}) for calcite (Millero, 1995). The saturation state of calcium carbonates (Ω) is thus controlled by the solubility product for calcite and the apparent thermodynamic constant K'_{sp}, which is a function of pressure, temperature, and salinity.

$$\Omega = \frac{Ca^{2+} \cdot CO_3^{2-}}{K'_{sp}} \tag{4}$$

Ca^{2+} denotes the concentration of dissolved calcium (see Section 2.2.2). While we acknowledge that our analyses may underrepresent the contributions of aragonite and dolomite to the benthic pool of $CaCO_3$, we are confident that the contribution of these minerals is minimal here based on literature data (e.g., Demina et al., 2020; Pautova et al., 2020; Solheim & Elverhoi, 1996). Calcite dissolution (Equation 5) and authigenic precipitation (Equation 6) are described by a kinetic-thermodynamic rate law with a linear dependency on saturation state (e.g., Morse, 1983):

$$R_{dissolution} = k_{diss} \cdot (1 - \Omega) \cdot CaCO_3 \quad \text{if } \Omega < 1 \tag{5a}$$

$$R_{dissolution} = 0 \quad \text{if } \Omega \geq 1 \tag{5b}$$

$$R_{precipitation} = k_{prec} \cdot (\Omega - 1) \quad \text{if } \Omega \geq 5 \tag{6a}$$

$$R_{precipitation} = 0 \quad \text{if } \Omega < 5 \tag{6b}$$

where the rate constants for calcite dissolution, k_{diss} and calcite precipitation k_{prec}, are taken from Luff et al. (2001). Our assumption of $\Omega \geq 5$ for calcite precipitation is based on experimental analyses (e.g., C. Zhang et al., 2010; Morse et al., 2003). These have shown that calcite precipitation rates increase at high Ω values due to greater availability of reactants (C. Zhang et al., 2010).

2.2.2. Boundary Conditions

Boundary conditions at the SWI are constrained by observed concentrations and assumed to be at steady state. Such a simplifying assumption is supported by our previous assessments (Freitas et al., 2020) where by using a steady-state RTM we were able to successfully describe and quantify long-term trends (ca. 2,000 years) in OM dynamics (Supporting Information S1). A no-flux condition is specified for all species at the lower boundary, here 100 cm depth (for details see Freitas et al., 2020). We use observational data to define species concentrations at the SWI by applying identical boundary conditions to Freitas et al. (2020). Additionally, we adopt site-specific pH values at the SWI determined during a cruise in summer 2018. At stations B14–B17 (Tables 1 and S2 in Supporting Information S1), downcore porewater pH was determined onboard using a punch-in pH probe (Thermo Scientific Orion Star A329; accuracy 0.002 pH units), which was calibrated prior to measurements at each site with standard solutions (pH 4.0, 7.0, and 10.0). The depth resolution is 0.5 cm between 0 and 2 cm depth, and 1.0 cm between 2 and 10 cm depth. Since no data are available for B13, a pH value is prescribed for that site following initial sensitivity tests of initial pH values and $CaCO_3$ dissolution rates. Here, we apply a conservative TA of 2,350 µM for all sites (Table 1), which is well in the general range found in the Barents Sea shelf when disregarding extreme/uncertain values determined by Hulth et al. (1996). In addition, we also run simulations assuming transient dynamics in the TA boundary condition to test if such bottom water transients would result in significantly different TA depth profiles and fluxes across the SWI (not shown). However, results show that a temporal variability in bottom water TA exerts a negligible effect. Instead, we run a steady-state model ensemble over the entire range of plausible TA and pH upper boundary conditions to quantify uncertainties in flux estimates (Section 2.2.5).

Concentrations of H_2CO_3, HCO_3^-, CO_3^{2-}, $B(OH)_3$, and $B(OH)_4^-$ at the SWI were calculated based on initial pH and TA (Table 1), and corrected for temperature, salinity, and water depth, according to Millero (1995) (Equation 7–15):

$$DIC_{up} = \frac{(TA_{up} + a) \cdot b}{c} \tag{7}$$

$$a = -\frac{k_{eq4} \cdot TB_{up}}{H^+ + k_{eq4}} - \frac{k_{eq3} \cdot TS_{up}}{H^+ + k_{eq3}} - \frac{k_{eq5}}{H^+} + H^+ \tag{8}$$

$$b = 1 + \frac{k_{eq1}}{H^+} + \frac{k_{eq1} + k_{eq2}}{(H^+)^2} \tag{9}$$

$$c = \frac{k_{eq1}}{H^+} + \frac{2 \cdot k_{eq1} \cdot k_{eq2}}{(H^+)^2} \tag{10}$$

where TA_{up} denotes TA given in Table 1. DIC_{up}, TB_{up}, and TS_{up} represent SWI carbonate alkalinity, borate alkalinity, and sulfide alkalinity, respectively. We assume TB_{up} of 425 µM and TS_{up} equal zero. The equilibrium constants (k_{eq1} to k_{eq5}) are calculated according to Millero (1995). Thus,

$$CO_3^{2-} = \frac{TC_{up} \cdot k_{eq1} \cdot k_{eq2}}{(k_{eq1} \cdot k_{eq2}) + (k_{eq1} \cdot H^+) + (H^+)^2} \tag{11}$$

$$HCO_3^- = \frac{TC_{up} \cdot k_{eq1} \cdot H^+}{(k_{eq1} \cdot k_{eq2}) + (k_{eq1} \cdot H^+) + (H^+)^2} \tag{12}$$

$$H_2CO_3 = DIC_{up} - HCO_3^- - CO_3^{2-} \tag{13}$$

$$B(OH)_4^+ = \frac{TB_{up} \cdot H^+}{k_{eq4} + H^+} \tag{14}$$

$$B(OH)_3 = TB_{up} - B(OH)_4^- \tag{15}$$

Contents of $CaCO_3$ at the SWI are from Faust et al. (2020). Porewater Ca concentrations (here assumed to be Ca^{2+}) are from cruise JR16006 (for details see Faust et al., 2020; Freitas et al., 2020).

2.2.3. Controls on pH and Ω

We quantify the relative contributions of diagenetic reactions to changes in pH and Ω following Jourabchi et al. (2005) and Blouet et al. (2021). In short, the influence of each reaction on pH is governed by the mass action laws (Table S1) and fulfills the condition of electric neutrality:

$$\left.\frac{dH^+}{dt}\right|_i = \frac{t_a^i - (\chi_1 + 2\chi_2)\, t_c^i - t_s^i \sigma_1}{A_1} R^i \tag{16}$$

$$A_1 \equiv DIC\frac{\partial \chi_1}{\partial H^+} + 2DIC\frac{\partial \chi_2}{\partial H^+} + T_S\frac{\partial \sigma_1}{\partial H^+} + T_B\frac{\partial \beta_1}{\partial H^+} - \frac{K_3}{H^{+2}} - 1 \tag{17}$$

Where t_a^i, t_c^i, and t_s^i are the stoichiometric coefficients for the production or consumption of alkalinity, DIC, and total sulfide, respectively, by a given kinetic reaction i, with rate R^i. The terms χ_1 and χ_2 are the relative contributions of HCO_3^- and CO_3^{2-} to DIC, respectively, β_1 is the relative contribution of $B(OH)_4^-$ to T_B, and σ_1 is the relative contribution of HS^- to T_S. χ_1, χ_2, σ_1, and β_1 are given by:

$$HCO_3^- = \chi_1 DIC$$

$$CO_3^{2-} = \chi_2 DIC$$

$$CO_2 = \chi_3 DIC$$

$$HS^- = \sigma_1 T_S \quad (18)$$

$$H_2S = \sigma_2 T_S$$

$$B(OH)_4^- = \beta_1 T_B$$

$$B(OH)_3 = \beta_2 T_B$$

and:

$$\chi_1 \equiv \frac{K_1^* H^+}{H^{+2} + K_1^* H^+ + K_1^* K_2^*}$$

$$\chi_2 \equiv \chi_1 \frac{K_2^*}{H^+}$$

$$\chi_3 \equiv 1 - \chi_1 - \chi_2$$

$$\sigma_1 \equiv \frac{K_4^*}{K_4^* + H^+} \quad (19)$$

$$\sigma_2 \equiv 1 - \sigma_1$$

$$\beta_1 \equiv \frac{K_5^*}{K_5^* + H^+}$$

$$\beta_2 \equiv 1 - \beta_1$$

Following Blouet et al. (2021) and Jourabchi et al. (2005), the contribution of a given reaction to changes in saturation state with respect to calcite Ω (Equation 4) can be expressed as a function of their contribution to the production or consumption of calcium and carbonate ions:

$$\left.\frac{d\Omega}{dt}\right|_i = \frac{1}{K'_{sp}} \left[CO_3^{2-} \left.\frac{dCa^{2+}}{dt}\right|_i + Ca^{2+} \left.\frac{dCO_3^{2-}}{dt}\right|_i \right] \quad (20)$$

The production or consumption of calcium and carbonate ions can then be expressed as a function of the previously derived rate of change in proton concentrations (Equation 16):

$$\left.\frac{d\Omega}{dt}\right|_i = \frac{1}{K'_{sp}} \left[CO_3^{2-} \left.\frac{dCa^{2+}}{dt}\right|_i + Ca^{2+} \left(t_c^i \chi_2 R^i + T_C \frac{\partial \chi_2}{\partial H^+} \left.\frac{dH^+}{dt}\right|_i \right) \right] \quad (21)$$

Note that since only calcite dissolution and precipitation impact the concentrations of Ca^{2+}, $\frac{dCa^{2+}}{dt}$ is zero for all other reactions.

2.2.4. Benthic-Pelagic Fluxes of DIC and Alkalinity

Steady-state benthic fluxes of DIC ($J_{DIC,Total}$) and TA ($J_{TA,Total}$) are calculated based on integrating the reaction rates that contribute DIC and TA to the porewaters over depth (e.g., Krumins et al., 2013; Table S1). These estimates account for the effects of all transport (advection, molecular diffusion, bioturbation, and bioirrigation) and reaction processes implemented in our RTM (Supporting Information S1; Freitas et al., 2020), and thus are equivalent to total benthic exchange at the SWI (Krumins et al., 2013). In addition, they allow assessing the significance of each biogeochemical process for producing/consuming TA and DIC. These findings provide valuable information for estimating the impacts of specific diagenetic processes on carbonate dynamics at the seafloor, which would be impossible to assess by using methods relying on concentration gradients at the SWI (e.g., Fick's law).

The benthic fluxes of DIC (Equation 22) and TA (Equation 23) are given by:

$$J_{DIC,Total} = J_{DIC,OM} + J_{DIC,Diss} + J_{DIC,Prec} \quad (22)$$

$$J_{TA,Total} = J_{TA,OM} + J_{TA,Diss} + J_{TA,Prec} + J_{TA,H2S} + J_{TA,Fe2+} + J_{TA,Mn2+} + J_{TA,NH4} \quad (23)$$

where the subscript terms OM, $Diss$, $Prec$, H_2S, Fe^{2+}, Mn^{2+}, and NH_4 correspond to OM degradation (primary redox reactions), dissolution (calcite and iron sulfide), precipitation of carbonates (calcium, manganese, and iron) and pyrite, sulfide oxidation, iron oxidation, manganese oxidation, and ammonium oxidation, respectively. The relative contributions of each process to DIC and TA fluxes (i.e., stoichiometry and direction—Consumption vs. production) are given in Table S1.

2.2.5. Sensitivity Analyses

There is a certain degree of uncertainty associated with pH, DIC, and TA concentrations of present and future bottom water and sedimentary porewater in the Barents Sea shelf. Further, it is generally unclear how the carbonate chemistry of bottom waters effectively impacts benthic fluxes of DIC and TA (e.g., Gazeau et al., 2014). Therefore, to explore the response of benthic carbonate fluxes to poorly constrained bottom water pH, DIC, and TA, we run a steady-state model ensemble over the entire range of plausible pH and TA conditions. We investigate how fluxes change under varying bottom water conditions and use these results to discuss the potential impact of projected future change on benthic fluxes. We cover a pH interval of 7.0–8.0, which is representative of pH values for the western Barents Sea shelf region (e.g., Husum et al., 2020; Kostka et al., 1999; Tessin et al., 2020; this study). Similarly, we explore a TA range of 2,000–2,700 μM, which covers bottom waters and surface sediment values reported for the Barents Sea and Svalbard shelves (Hulth et al., 1996), as well as for the East Siberian Shelf (Miller et al., 2017). All other site-specific model parameters and boundary conditions follow baseline values (Freitas et al., 2020).

Further, using a similar approach employed in our previous work (März et al., 2022), we explore how the effect of changes in OM deposition fluxes at the SWI may impact carbonate dynamics at the seafloor. We emphasize that our sensitivity tests are limited to just a few factors because the model has already been carefully calibrated and validated for the present-day dynamics on the basis of a comprehensive porewater and sediment data set (Freitas et al., 2020) and it is beyond our scope to explore the response of benthic fluxes to the full range of projected environmental change. Here, we select sedimentation rates, OM, metal oxide, and calcite to offer a first-order estimate of how the benthic carbonate system may respond to changes in these input fluxes. More specifically, from our baseline conditions (this work; Freitas et al., 2020; März et al., 2022), we test the following cases at each site: 2x sedimentation rates; 0.5x and 2x OM; 0.5x and 2x calcite; 0.5x and 2x metal oxides. We use these outputs to assess the impact on rates of dissolution and precipitation, as well as benthic fluxes of DIC and TA.

3. Results and Discussion

3.1. Inorganic Carbon and pH Dynamics Along the Barents Sea 30°E South-North Transect

Overall, our model results agree well with the observed downcore evolution of measured pH values, as well as $CaCO_3$ contents and porewater Ca^{2+} concentrations (Figure 3). Slight mismatches between observed and simulated Ca^{2+} concentrations at sites B13 and B17 may result from slight underestimation of carbonate dissolution rate constants, which are derived from Luff et al. (2001) or from the assumed saturation threshold ($\Omega \geq 5$) (see below). Furthermore, at site B17 the disagreement could also come from the assumed bottom water Ca^{2+} concentrations (Table 1). Because bottom water pH has not been measured at site B13, we tested if a lower bottom pH might drive a more intense carbonate dissolution in the upper layer but found that the effect is limited and does not improve the fit. Alternatively, the mismatch may arise from processes not explicitly resolved in our model (see below).

Observations and simulation results reveal a common pattern in benthic carbonate dynamics. Across the entire transect, the upper, well mixed sediment layers (<5 cm) are characterized by low pH and undersaturation of porewaters with respect to calcite, followed by an increase in porewater pH and calcite oversaturation deeper in

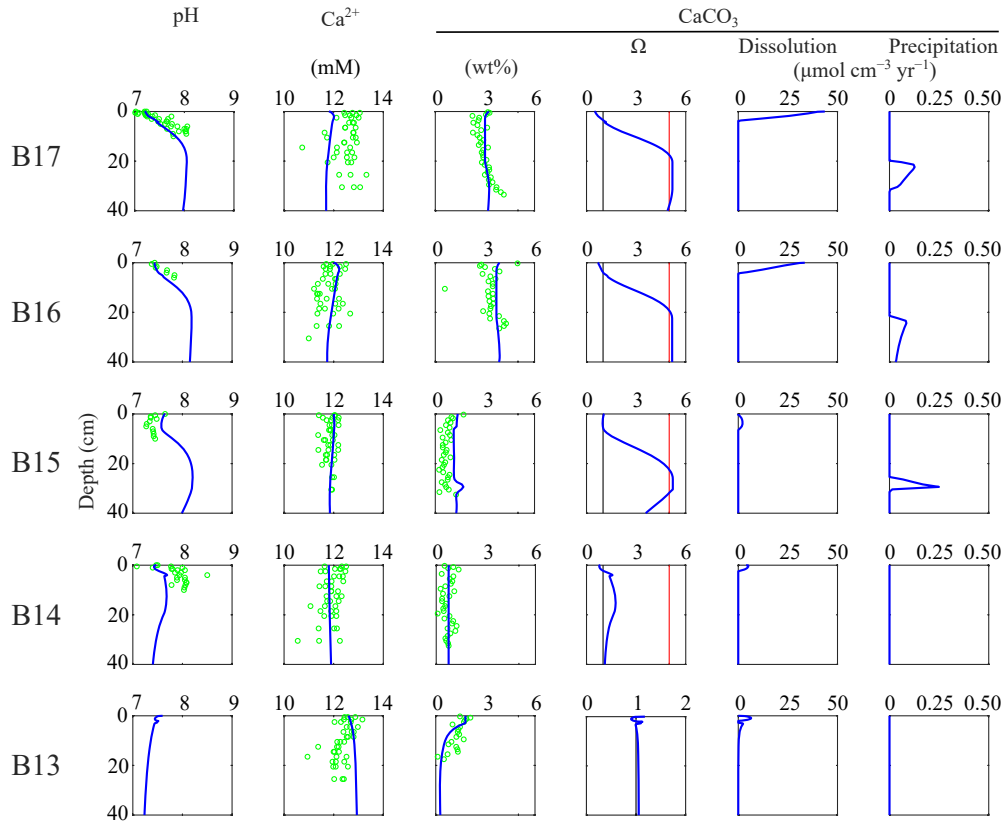

Figure 3. Evolution of pH and carbonate system parameters with sediment depth (in cm) along a 30°E transect in the Barents Sea. Blue lines represent model outputs. Black line on CO_3^{2-} denotes carbonate ions equilibrium. Black and red lines on Ω panels denote calcium carbonate saturation (Ω = 1) and saturation threshold (Ω ≥ 5), respectively. Green circles represent observations (see text for references).

the sediments. However, the level of porewater over- and undersaturation, and thus carbonate dissolution and precipitation rates reveal a geographical trend, with decreasing rates from north to south.

At the northern part of the transect (B16–B17), bottom waters are characterized by low pH (pH < 7.45) and undersaturation with respect to calcite (Ω = 0.48–0.68). The shallowest sediment layers reveal high carbonate dissolution rates (Equation 5; $R_{dissolution} > 25$ μmol cm^{-2} yr^{-1} at the SWI) which coincide with an increase in Ca^{2+} concentrations and a decrease in $CaCO_3$ contents close to the SWI (Figure 3). At the southern part of the transect (B13–B15), bottom water pH (pH > 7.45) and saturation state (Ω ≈ 1) are higher, but benthic carbonate contents are lower than in the northern part stations (Figure 3). Consequently, upper sediment carbonate dissolution is approximately 10-fold lower.

The S—N trend in the intensity of porewater undersaturation and dissolution rates is mirrored by the intensity of porewater oversaturation and carbonate precipitation rates below the well-mixed layer. At the northern part of the transect (B16–B17), porewater pH and Ω increase downwards to broad mid-core (10–20 cm) maxima of pH > 8.0 and Ω > 5, while the southern part of the transect (B13–B14) reveals increasingly lower and more localized mid-depth (5–20 cm) pH and Ω maxima of pH = 7.4–7.6 and Ω = 1.0–1.7. At the southernmost station (B13), porewater pH decreases from 7.6 at the SWI with only a very weakly pronounced and very narrow reversal around 2 cm depth (Figure 3). Porewater calcite saturation thus remains relatively constant, close to unsaturated conditions throughout the simulated sediment column due to a near-complete consumption (i.e., dissolution) of the low sediment carbonate contents and the resulting decrease in buffering capacity. Thus, unfavorable conditions for carbonate precipitation prevail, following our assumption of Ω ≥ 5 to enable authigenic calcite precipitation. This finding could explain some of the mismatch between model results and analytical data for Ca^{2+}. Further, this mismatch could be explained by authigenic precipitation of carbonate fluorapatite (CFA). CFA precipitation consumes porewaters Ca^{2+} (Ruttenberg, 2014; Zhao et al., 2020) and could explain the gradual

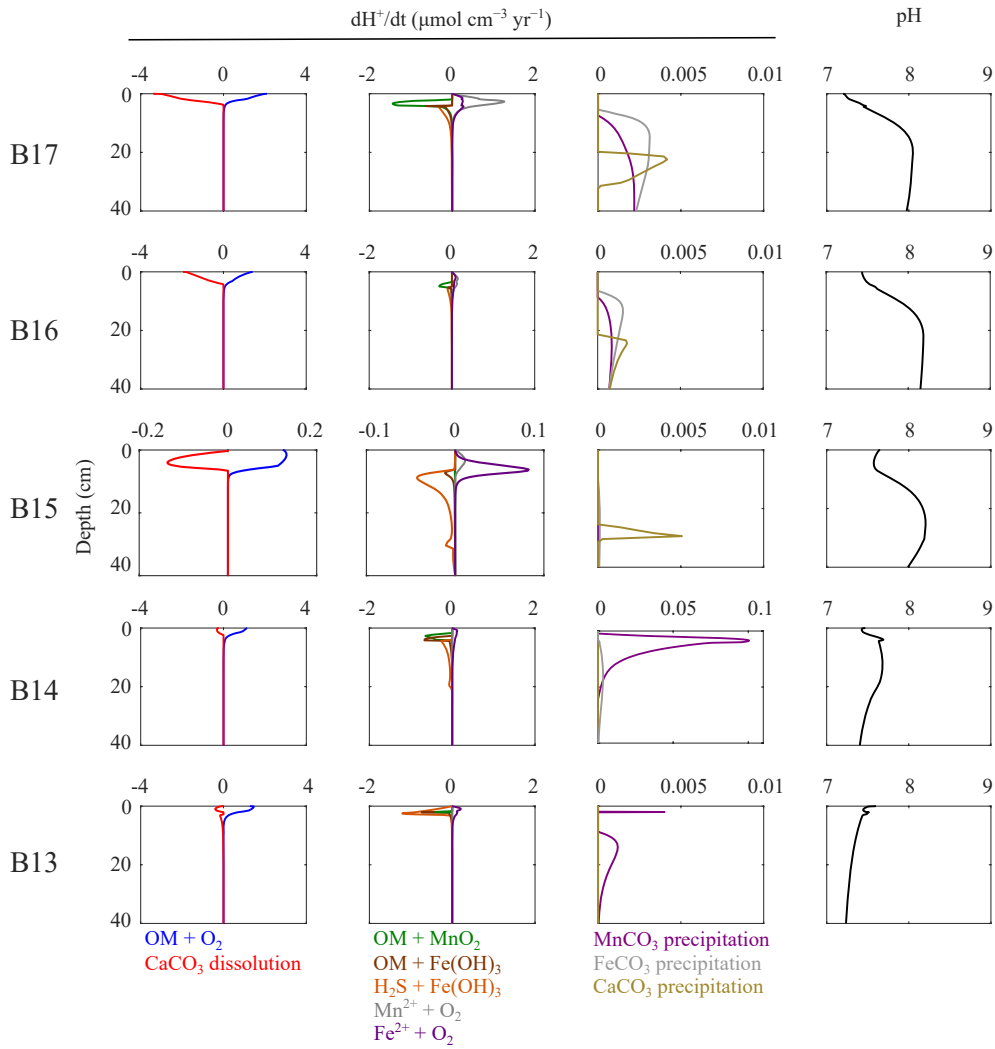

Figure 4. Biogeochemical processes controlling sedimentary evolution of pH with depth. Note that rates of proton production (consumption) (Equation 16) result in a decrease (increase) in porewater pH (Blouet et al., 2021).

downcore decrease we recorded in measured Ca^{2+} in site B13. However, our model does not explicitly resolve CFA and its impact on Ca^{2+}depth profiles. Here, we can only infer CFA precipitation based on our porewater phosphate (Freitas et al., 2020), which reach an asymptotic profile at ≤10 μM (e.g., Slomp et al., 1996).

Rates of authigenic carbonate precipitation are two orders of magnitude lower than those of dissolution; therefore, model-derived authigenic carbonate precipitation only modestly affects Ca^{2+} and $CaCO_3$ contents at depth. We assess the impact of the Ω threshold on precipitation, and thus precipitation rates, on simulated benthic profiles by assuming a threshold of $\Omega \geq 1$ for authigenic precipitation (Figure S1 in Supporting Information S1). Although these test results lead to a significant increase in precipitation, they also produce further mismatches between model and data depth profiles (Figure S1). Thus, we maintain our relatively conservative threshold of $\Omega \geq 5$ (Section 2.2.1; C. Zhang et al., 2010; Morse et al., 2003) for authigenic carbonate precipitation.

3.2. Main Drivers of Inorganic Carbon and pH Dynamics Along the Barents Sea 30°E Transect

Within the upper, well-mixed sediment layers (<5 cm), pH and Ω dynamics are mainly driven by the balance between aerobic degradation of OM and calcite dissolution (Figures 4 and 5). This is a typical feature of oxic marine sediments, where aerobic OM degradation induces acidification of porewaters, and leads to metabolic dissolution of calcite (Adler et al., 2001; Berelson et al., 1990; 1994; Emerson & Archer, 1990; Hales et al., 1994;

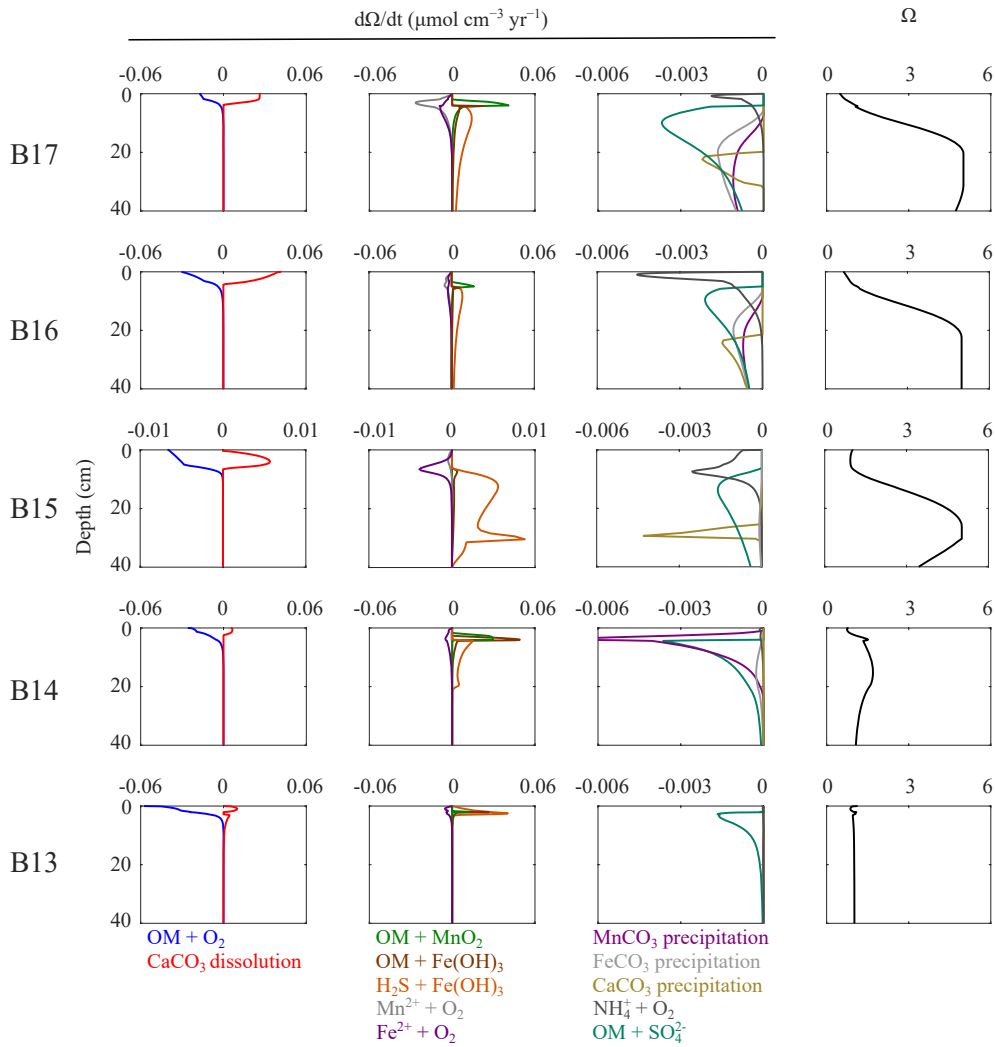

Figure 5. Biogeochemical processes controlling sedimentary evolution of Ω with depth.

Hulth et al., 1994; Jahnke et al., 1994; 1997; Jahnke & Jahnke, 2000; 2004). Whether the interplay of these two opposing processes results in a decrease or increase in upper sediment pH and Ω is mainly determined by the saturation state of bottom waters. At the northern sites (B16–B17), the deposition of very reactive OM (see Freitas et al., 2020) supports the highest aerobic OM degradation and proton production rates (1–2 μmol H^+ cm^{-3} (porewater) yr^{-1}; Figure 4). Since corrosive bottom waters (pH < 7.45; Ω < 1) further enhance calcium carbonate dissolution in the upper sediment and calcite contents are not limiting ($CaCO_3$ > 3 wt%) in this part of the Barents Sea (Faust et al., 2020), the positive effect of calcium carbonate dissolution rates on pH and Ω exceeds the negative effect of aerobic OM degradation (Figure 5). In contrast, at the southernmost sites (B13–B15), higher bottom water pH (pH > 7.45), saturation of bottom waters with respect to calcium carbonate (Ω ≈ 1), and lower carbonate contents ($CaCO_3$ < 2 wt%; Faust et al., 2020) combine to limit the counterbalancing effect of carbonate dissolution on pH and Ω. Consequently, the high rates of aerobic OM degradation (Freitas et al., 2020) drive a shallow local minimum pH and Ω just below the SWI (Figures 4 and 5). In addition, at site B15, the exceptionally low reactivity of the depositing OM (Freitas et al., 2020) results in a less pronounced, yet more drawn out pH and Ω minimum.

When oxygen (and nitrate) becomes depleted in the porewaters, Mn or Fe (oxyhydr)oxide pathways of OM degradation replace aerobic metabolisms and trigger a reversal in pH and Ω profiles (Berner et al., 1970; Canfield et al., 1993; Hu & Cai, 2011; Kostka et al., 1999; Tessin et al., 2020). Accordingly, we find that below the mixed layer (5–10 cm), metal oxide reduction exerts an important control on pH and Ω despite their modest

contributions toward overall OM degradation rates (<11%; Freitas et al., 2020). Often in combination with the oxidation of sulfide by iron (oxyhydr) oxides, the metal oxidation pathways consume H^+ (with maxima rates of −1.0 to −0.5 μmol cm^{-3} yr^{-1} of H^+), thus increasing pH values (Figure 4). These processes produce local pH maxima and drive porewaters to oversaturation. The impacts of metal oxide pathways on both pH and Ω are largest at sites B13, B14, B16, and B17. These sites are characterized by the deposition of high reactivity OM (Freitas et al., 2020; Stevenson & Abbott, 2019), which supports high rates of OM degradation (Figure 2; Freitas et al., 2020). At site B15, sulfide oxidation by iron (oxyhydr) oxides also drives pH and Ω maxima; however, the rates of change are comparatively lower in this station due to generally lower rates of OM degradation (Figure 2; Freitas et al., 2020).

At the northern sites, positive changes in Ω are sufficiently large to meet the empirically found threshold of $\Omega \geq 5$ (e.g., C. Zhang et al., 2010; Morse et al., 2003). Thus, Ω oversaturation driven by calcite metabolic dissolution and metal oxide pathways (see above) enables authigenic carbonate precipitation ($\Omega > 5$) at 25–40 cm (Figures 3 and 5). By contrast, at site B17, reoxidation of Mn^{2+} and Fe^{2+} by O_2 results in proton production (Cai et al., 2000; Cai & Reimers, 1993; Forja et al., 2004; Jourabchi et al., 2005; Soetaert et al., 2007) and drive a subsurface negative shift in Ω (−0.02 years^{-1}). Nevertheless, H^+ increase is buffered by proton consumption through calcite dissolution and metal oxides reduction.

In deeper sediment layers (>10 cm), authigenic precipitation of carbonate minerals ($MnCO_3$, $FeCO_3$, and $CaCO_3$) results in proton production, and thus a drop in pH (Jourabchi et al., 2005; Soetaert et al., 2007). Consequently, Ω also decreases in response to authigenic precipitation. However, because process rates are 1–2 orders of magnitude slower than those of the processes outlined above, authigenic carbonate precipitation only represents a minor control on pH and Ω within the investigated sediment depths, and total amounts of authigenic carbonate are likely negligible. OSR and nitrification further drive negative changes in Ω. However, the effect these processes in Ω shifts are of relatively minor importance (Figure 5).

In summary, our model results confirm the expected patterns of diagenetic controls on pH and carbonate dynamics at the seafloor (Jourabchi et al., 2005; Krumins et al., 2013; Morse, 1983; Soetaert et al., 2007). In particular for the Barents Sea shelf, our assessments reveal that benthic carbonate dynamics are mainly controlled by a combination of bottom water conditions (pH, Ω, and calcite availability) and OM degradation within the sediment. Furthermore, we found that these patterns display a notorious S—N zonation, which somewhat contrasts our previous findings concerning OM transformation patterns (Freitas et al., 2020). At the northern sites, higher surface ocean pH values > 8.1 that only weakly decrease to 8.0 in waters deeper than 300 m (Jones et al., 2019) favor PIC export through the water column to the seafloor, resulting in the relatively high $CaCO_3$ contents preserved in those sediments (Faust et al., 2020). By contrast, the deposition of highly reactive OM supports high rates of aerobic OM degradation in the upper sediment layers, driving low pH conditions in both bottom waters (Steinsund & Hald, 1994) and sediment layers directly below the SWI (pH = 7.45–7.65; Freitas et al., 2020). The resulting metabolic dissolution of the deposited $CaCO_3$ results in efficient pH buffering and an increase in Ω, which is further promoted by metal oxide pathways (e.g., Jourabchi et al., 2005; Soetaert et al., 2007). These processes enable deeper authigenic carbonate precipitation at the northern sites. In contrast, at the southern-central parts of the transect, lower carbonate contents at the seafloor (Faust et al., 2020) in combination with equally high rates of aerobic OM degradation (Freitas et al., 2020) (except for site B15) drive a drop in porewaters pH relative to bottom waters pH at the SWI (pH < 7.45). Since calcite availability limits calcite dissolution (Figure 3), seafloor buffering capacity of porewaters never reaches saturation states that would allow for authigenic precipitation ($\Omega > 5$).

3.3. Benthic DIC and Alkalinity Fluxes

Net benthic DIC fluxes from the sediment into the overlying water column range from 12.5 to 59.5 μmol cm^{-2} yr^{-1} and display a clear S–N difference (Figure 6). Relatively lower $J_{DIC,Total}$ are calculated for the southern-central sites (B13–B15), while higher DIC effluxes are quantified at the northern B16–B17 areas ($J_{DIC,Total}$ > 50 μmol cm^{-2} yr^{-1}). At B13–B15, DIC fluxes are predominantly supported by heterotrophic OM degradation (mostly aerobic OM degradation and OSR; Figure S2 in Supporting Information S1), while at the northern areas, calcite dissolution further enhances the OM degradation-driven DIC flux and supports nearly one-third of $J_{DIC,Total}$ ($J_{DIC,Diss}$ = 20.1–21.9 μmol cm^{-2} yr^{-1}). At B16–B17, authigenic carbonate precipitation deeper in the sediments

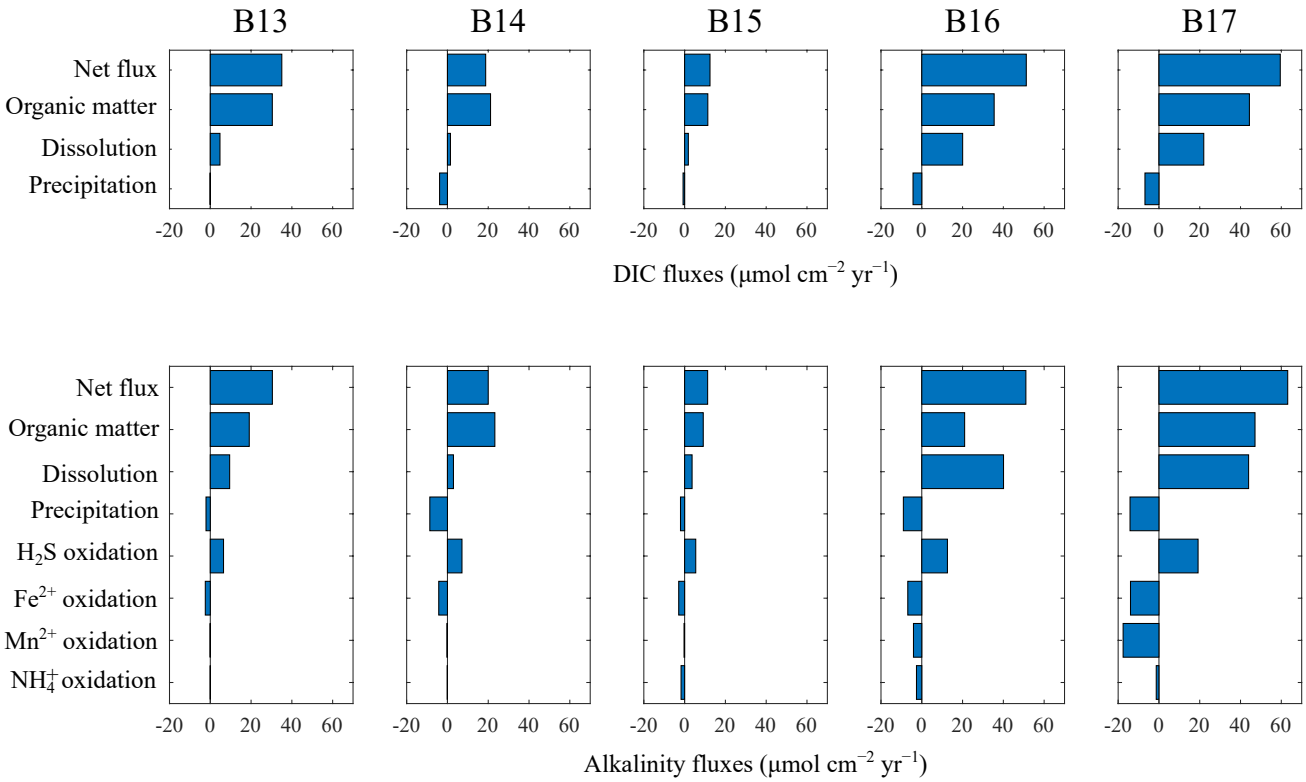

Figure 6. Benthic effluxes of alkalinity (bottom row) and dissolution of inorganic carbon (DIC) (top row) derived from representative scenarios for Barents Sea. Fluxes are given as total net fluxes across the sediment-water interface (positive at all sites), and these are further partitioned by the contribution of each diagenetic process to production (positive values) and consumption (negative values) of alkalinity and DIC.

acts as a DIC sink ($J_{DIC,Prec} = -3.8$ to -6.8 μmol DIC cm^{-2} yr^{-1}). Yet, this only exerts a small effect on DIC fluxes.

Overall, benthic DIC production at the Barents Sea shelf sediments (ca. 300 m depth) is one order of magnitude lower than DIC production predicted for low latitude, shallow shelf (25–150 m depth) environments at a global scale (Krumins et al., 2013). This difference can mainly be explained by contrasting environmental conditions, as well as distinct model parametrizations between Freitas et al. (2020) and Krumins et al. (2013). Krumins et al. (2013) do not explicitly resolve authigenic calcite precipitation, thus neglecting an important DIC sink at a global scale and potentially overpredicting DIC fluxes. In addition, the applied models differ in both OM degradation description and the magnitude and reactivity of the applied OM flux. While Krumins et al. (2013) apply a 1G model for OM degradation, thus assuming a constant reactivity with sediment depth, Freitas et al. (2020) describe OM degradation by the means of the reactive continuum model, thus accounting for the widely observed decrease in OM reactivity with depth. For the Barents Sea sites, the magnitude and reactivity of the OM deposition flux are constrained on the basis of comprehensive, site-specific observational data. The apparent OM reactivity k at the SWI determined by Freitas et al. (2020) ranges between 4.5×10^{-3} and 2.0×10^{-2} yr^{-1}, and rapidly decreases to $k < 10^{-4}$ yr^{-1} with burial depth/time. OM degradation and DIC production thus decrease with depth. In contrast, the model of Krumins et al. (2013) is parametrized based on global data (Thullner et al., 2009) and they assume a large OM flux (2.32–6.46 mol C m^{-2} yr^{-1}) of highly reactive OM (first order degradation rate, $k = 0.1$–1.0 years^{-1}). These idealized global coastal ocean conditions result in the large DIC fluxes.

Net TA benthic fluxes mirror the simulated DIC pattern (Figure 6), that is, with higher $J_{TA,Total}$ at the northern sites ($J_{TA,Total} = 51.1$–63.2 μmol cm^{-2} yr^{-1}) than in the southern areas ($J_{TA,Total} = 11.3$–30.4 μmol cm^{-2} yr^{-1}). At B13–B15, heterotrophic OM degradation represents the main source of alkalinity (predominantly from OSR; Figure S2 in Supporting Information S1). Additionally, calcite dissolution and sulfide oxidation by iron (oxyhydr) oxides further add to the TA pool. By contrast, carbonate and pyrite precipitation, as well as aerobic iron oxidation only consume minor amounts of TA. At the northern sites, calcite dissolution plays a much larger role in

producing alkalinity ($J_{TA,Diss}$ = 40.1–43.9 μmol cm^{-2} yr^{-1}). At B17, calcite dissolution nearly contributes as much as OM degradation to the TA production/flux. At B16, the contribution of calcite dissolution to the TA production/flux is 2-fold higher than OM degradation. Sites B16 and B17 are characterized by lower pH values at the SWI (pH < 7.45), high rates of aerobic OM degradation, and high calcite contents (Sections 3.1 and 3.2). Altogether, these factors support higher rates of calcite dissolution, and thus TA production. Additionally, sulfide oxidation (by iron (oxyhydr) oxides) becomes more important for TA production ($J_{TA,H2S}$ = 12.6–19.2 μmol cm^{-2} yr^{-1}). In contrast, mineral precipitation ($J_{TA,Prec}$ = −9.0 to −14.2 μmol cm^{-2} yr^{-1}) and aerobic oxidation of dissolved manganese, iron, and ammonium ($J_{TA,Mn2+} + J_{TA,Fe2+} + J_{TA,NH4}$ = −13.5 to −32.8 μmol cm^{-2} yr^{-1}) consume large amounts of porewater alkalinity due to the higher relative contribution of these biogeochemical processes than at the southern sites. Site B17 (and B16 to a lesser extent) displays high rates of OM degradation (Figure 2), of which nearly half is coupled to MnO_2 reduction and OSR, resulting in high production rates of Mn^{2+} and HS^-. Here, sulfide oxidation is mostly coupled to iron (oxyhydr) oxide reduction, which produces Fe^{2+}. Further, the products Mn^{2+} and Fe^{2+} are oxidized by oxygen (Freitas et al., 2020).

To put the estimated TA fluxes for the Barents Sea in a wider context, we compiled available global benthic TA flux values from the coastal to the deep sea and covering a wide range of OM deposition fluxes (Table 2). By examining the flux estimates on Table 2 (and references therein) we find that: (a) global seafloor TA fluxes are highly variable and (b) simulated $J_{TA,Total}$ for the Barents Sea shelf falls at the lower end of globally observed values. The global variability can be explained by the different nature of the OM input, redox conditions in overlying waters and below the seafloor, and depositional rates. Additionally, methodologies vary, with in situ benthic chamber incubations being the most common way of deriving these fluxes (Table 2). Therefore, establishing meaningful comparisons with our estimates must be done with a certain degree of caution to account for these factors.

Overall, our estimated net $J_{TA,Total}$ values (11.3–63.2 μmol cm^{-2} yr^{-1}) are similar to TA fluxes determined for sites in (a) the productive, yet deep Equatorial Pacific (−13.9–48.7 μmol cm^{-2} yr^{-1}) (Berelson et al., 1990; 1994), (b) the Equatorial North Atlantic (−1.0–23.6 μmol cm^{-2} yr^{-1}), where sedimentary carbonate contents are generally high (Jahnke & Jahnke, 2004), as well as (iii) shelf and slope settings found along the California margin (Berelson et al., 1987; Jahnke et al., 1997) and the Gulf of Mexico (Berelson et al., 2019). These are deeper areas (>790 m) located within highly productive system and exposed to pelagic hypoxic conditions, thus experiencing acidification (Table 2). Similar order of magnitude TA fluxes are also reported for shallow parts of the California margin (Monterey Bay – 100 m depth) experiencing periods of low pelagic productivity, thus decreased OM degradation rates and sediment nutrient efflux (Berelson et al., 2003). Although the characteristics of the depositional environments vary, these are all sites that receive highly reactive OM and are often bathed in corrosive bottom waters.

By contrast, our $J_{TA,Total}$ estimates are one order of magnitude lower than model-derived, global values for idealized coastal and shelf sediments (Krumins et al., 2013). Similar to DIC flux estimates, such differences can be explained by differences in environmental conditions (OM input and reactivity) and model assumptions and parametrizations in our present work (and Freitas et al., 2020) and the global-scale assessments (Krumins et al., 2013). Furthermore, $J_{TA,Total}$ values for the Barents Sea are significantly lower than TA fluxes for near coast environments, such as the Rhone delta, where the anaerobic oxidation of methane results in high TA production (Rassmann et al., 2020), as well as at estuarine systems in SW Spain (Forja et al., 2004) and the coast of the Gulf of Mexico (Berelson et al., 2019). These areas receive high loads of terrestrial and fluvial OM inputs that quickly accumulate in the sediment.

3.4. Sensitivity of Seafloor Carbonate Dynamics to Varying Environmental Conditions

Since projected changes in sea-ice and progressive Atlantification (Årthun et al., 2012; Barton et al., 2018; Carmack & Wassmann, 2006; Oziel et al., 2020; Smedsrud et al., 2013) may represent further stressors for seafloor inorganic carbon dynamics, we developed a series of sensitivity experiments (Section 2.2.5) to explore the sensitivity of seafloor DIC and TA fluxes to possible future changes in environmental conditions. These are not specific projected scenarios for the Barents Sea and our assessments are designed to illustrate the potential mechanistic response of the carbonate system in the Barents Sea seafloor to changes in bottom water pH and

Table 2
Compilation of Benthic TA Fluxes Across Contrasting Marine Systems

Site	Setting	Depth (m)	OM input	TOC (wt%)	Type	J_{TA}	Unit	Reference
Barents Sea	Shelf	290–355	Pelagic	1.8–2.5	Model (Steady state)	11.3–63.2	μmol cm^{-2} yr^{-1}	This study; Freitas et al. (2020)
Global	Coast—Shelf	25–150	Pelagic	2.3–6.4 mol C m^{-2} yr^{-1} (OM flux at the SWI)	Model (Steady state)	200.7–616.8	μeq cm^{-2} yr^{-1}	(Krumins et al., 2013)
Equatorial Pacific	Abys	4,450–4,910	Pelagic	0.5–1.0	Chamber (total)	−13.9–36.7	μeq cm^{-2} yr^{-1}	Berelson et al. (1990); Jahnke et al. (1982)
Equatorial Pacific	Abys	3,380–4,560	Pelagic	0.2–1.0	Chamber (total)	13.5–47.8	μeq cm^{-2} yr^{-1}	Berelson et al. (1994); Hammond et al. (1996)
Cape Verde Plateau	Abys	3,103	Pelagic	n.a.	Chamber (total)	−1.0–11.0	μeq cm^{-2} yr^{-1}	Jahnke and Jahnke (2004)
Ceara Rise	Abys	3,272–4,676	Pelagic	n.a.		−12.9–23.6		
North Carolina depocenter	Slope	750–2,937	Pelagic and lateral transport	1.4–2.7	Chamber (total)	43.3–392.3	μeq cm^{-2} yr^{-1}	Jahnke and Jahnke (2000)
California margin	Slope	790–3,745	Pelagic and episodic lateral transport[d]	2.9–3.5	Chamber (total)	54.7–113.2	μeq cm^{-2} yr^{-1}	Jahnke et al. (1997); Jahnke et al. (1990)
Southern California	Shelf	900–1,800	Pelagic and episodic lateral transport	3.5–6.0	Chamber (total)	61.7–68.3	μeq cm^{-2} yr^{-1}	Berelson et al. (1987)
Monterey Bay – California	Shelf	100	Pelagic (upwelling)	0.4–0.5	Chamber (total)	74.8–333.2	μeq cm^{-2} yr^{-1}	Berelson et al. (2003)
Gulf of Mexico	Coast	16–30	Mixed pelagic and terrestrial	1.5–1.7	Chamber (total)	240.9–2,701	μeq cm^{-2} yr^{-1}	Berelson et al. (2019); Waterson and Canuel (2008)
	Shelf—Slope	130–1.550	Mainly pelagic Minor terrestrial	0.8–1.3		69.4–219.0		Morse and Beazley (2008)
Rhone delta	Coast—Shelf	20–72	Mixed pelagic and terrestrial	1.3–2.0	Chamber (total)	135.1–2,697	μmol cm^{-2} yr^{-1}	Rassmann et al. (2020)
Tomales Bay – California	Estuary	3–6	Pelagic with terrestrial	n.a.	Chamber (total)	138.7–521.9	μeq cm^{-2} yr^{-1}	Smith et al. (1987); Dollar et al. (1991)
Tinto—Odiel System	Estuary	2–5	Mainly terrestrial (inc. anthropogenic) and aquatic	1.1–2.4	Chamber (total)	−10,004–12,592	μmol cm^{-2} yr^{-1}	Ortega et al. (2008)
Ria de Vigo	Estuary	4–20	Mainly terrestrial (inc. anthropogenic) and aquatic	2.9–6.9	Chamber (total)	4,307–7,516	μmol cm^{-2} yr^{-1}	Forja et al. (2004)
Bay of Cadiz		2–14		2.0–2.9		3,869–5,329		
Odiel Estuary		3–8		1.9–4.2		3,613–5,073		
Barbete Estuary		3		1.7		4,854		
Palmones Estuary		2–5		0.9–3.4		3,577–4,964		

Note. n.a., data not available; TOC, total organic carbon.

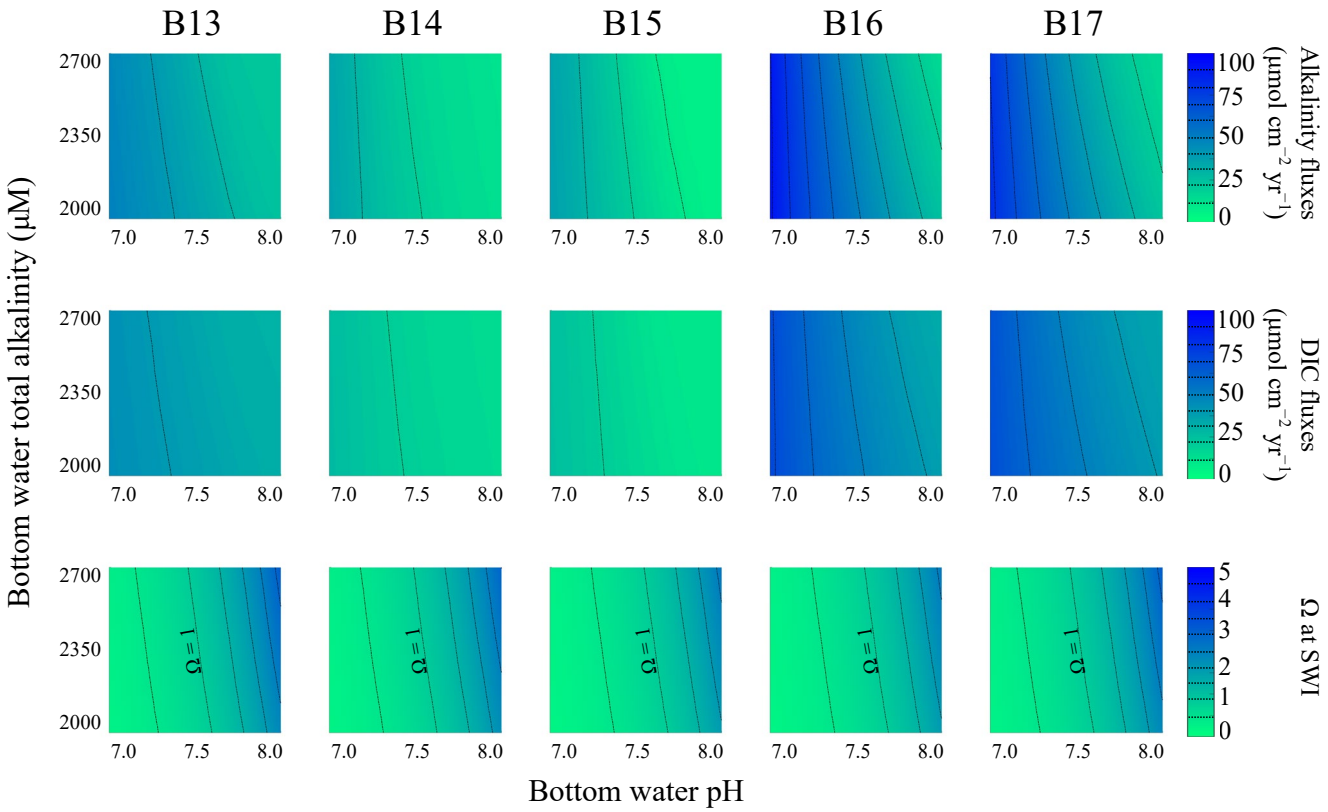

Figure 7. Sensitivity of carbonate chemistry parameters at the seafloor relative to changes in bottom water pH (horizontal axis) and total alkalinity (vertical axis): top row, benthic alkalinity effluxes ($J_{TA,Total}$); middle row, benthic dissolution of inorganic carbon (DIC) effluxes ($J_{DIC,Total}$); bottom row, Ω at the sediment-water interface (SWI).

alkalinity (Section 3.4.1), as well as OM deposition (Section 3.4.2) that have been shown to exert the main control on DIC and TA cycling in the Barents Sea.

3.4.1. Bottom Water pH and Alkalinity

Despite the plausible range of bottom water TA explored here (e.g., Hulth et al., 1996; Miller et al., 2017), we see that the impact of variations in bottom water TA on both TA and DIC fluxes (Figure 7) is generally low (the isolines are nearly vertical). This suggests that global seafloor TA fluxes are highly variable and the uncertainties in applied bottom water TA concentrations have a negligible influence on TA flux estimates. By contrast, along the studied range of pH conditions, we observe far more prominent changes in benthic TA and DIC effluxes. Generally, the highest TA and DIC fluxes, reaching nearly 100 µmol cm^{-2} yr^{-1} at the northern sites are simulated for more corrosive bottom water conditions with a pH = 7.0. These trends in $J_{TA,Total}$ and $J_{DIC,Total}$ are further supported by changes in Ω at the SWI (Figure 7). Saturation state largely falls below one at bottom water pH < 7.6, although this threshold gradually shifts to pH < 7.5 at greater bottom water total alkalinity (TA > 2,600 µM).

Our model results highlight the role of bottom water pH in further promoting shallow calcium carbonate dissolution and supporting higher DIC and TA fluxes. They agree with laboratory-based experiments which show that low bottom water pH conditions (pH = 7.1) produce large TA effluxes (Gazeau et al., 2014), and field observations that suggest bottom water pH < 7.3 promote carbonate dissolution at the SWI (Kostka et al., 1999). At pH = 8.0, net effluxes generally decrease but are higher at high bottom water alkalinity (TA > 2,350 µM).

Our sensitivity analyses of bottom water pH and TA further highlight the S–N patterns that we uncovered with our RTM approach. Our results suggest that bottom water acidification will have a more pronounced impact on the northern shelf (assuming that all other conditions remain unchanged) because B16–B17 are characterized by higher calcite contents (Faust et al., 2020), and thus more susceptible to corrosive conditions.

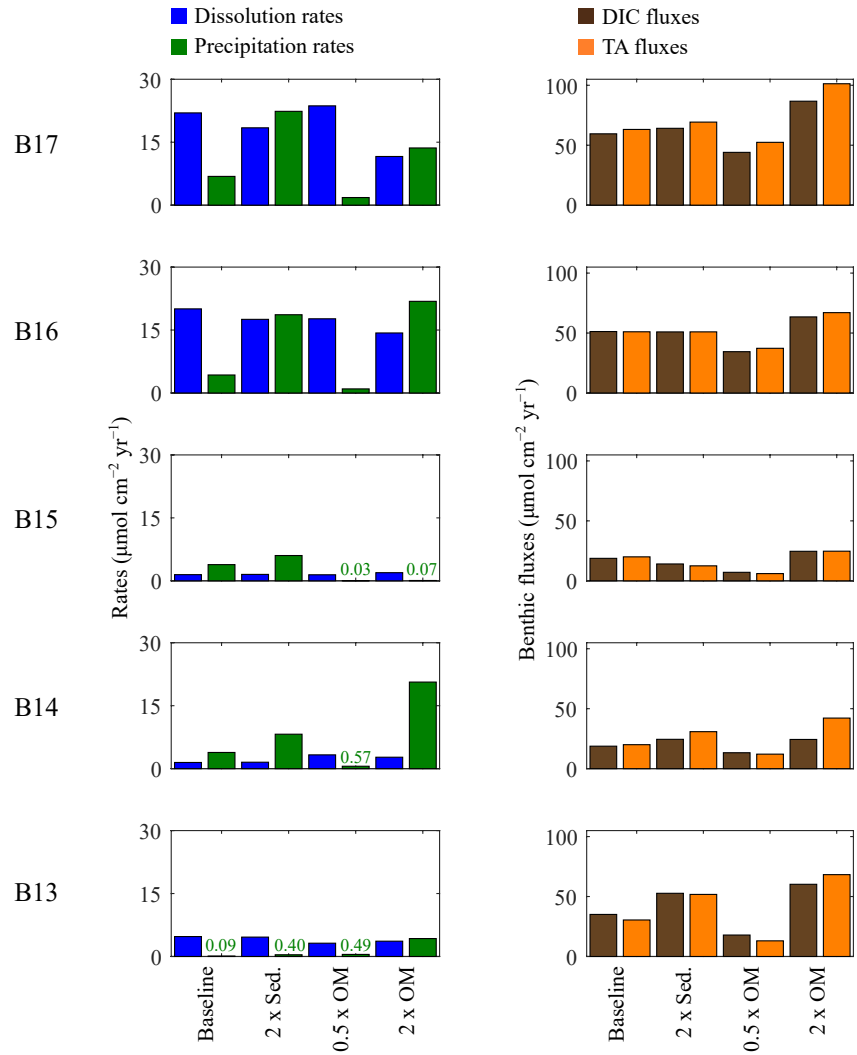

Figure 8. Sensitivity of seafloor carbonate chemistry parameters to changes in sedimentation rates (2x) and organic matter (OM) inputs (0.5x and 2x). Left column: rates of dissolution (blue) and precipitation (green). Right column: benthic fluxes of dissolution of inorganic carbon (DIC) (brown) and total alkalinity (TA) (orange).

3.4.2. Particulate Export to the Seafloor

Our model results also show that the quantity of OM and iron/manganese oxide deposition and, in particular, the resulting redox zonation of the sediment, and calcium carbonate contents (Section 3.2.2) exert further controls on TA and DIC benthic fluxes along the Barents Sea transect. It has been suggested that the projected loss of Arctic sea ice and associated circulation changes will prolong the ecological productive period and therefore have a fundamental impact on ecosystem structure (e.g., Lewis et al., 2020; Oziel et al., 2020). Although important, it remains difficult to predict future consequences on OM deposition fluxes. Thus, we explore how changes in deposition fluxes to the seafloor may impact carbonate dynamics (Figure 8; Table S3–S7). Similarly, it remains unclear how these changes may impact PIC delivery to the seafloor (e.g., Luo et al., 2016), as well as reactive metal oxide fluxes to the SWI. To address this gap, we also assess the impacts of shifts in input fluxes of metal oxides and PIC (Figure 9; Table S3–S7 in Supporting Information S1).

Depositional environments subject to high sedimentation rates are generally characterized by a rapid depletion of oxygen, thus favoring sub-oxic and anoxic metabolic pathways (Burdige, 2006; Middelburg, 2019), which can promote Ω oversaturation and authigenic calcite precipitation (Berner et al., 1970; Green & Aller, 2001; Hu & Cai, 2011; Rassmann et al., 2020). Accordingly, model results indicate that a general doubling in sedimentation rates lead to an increase in authigenic precipitation rates at all sites (Figure 8). However, the magnitudes of

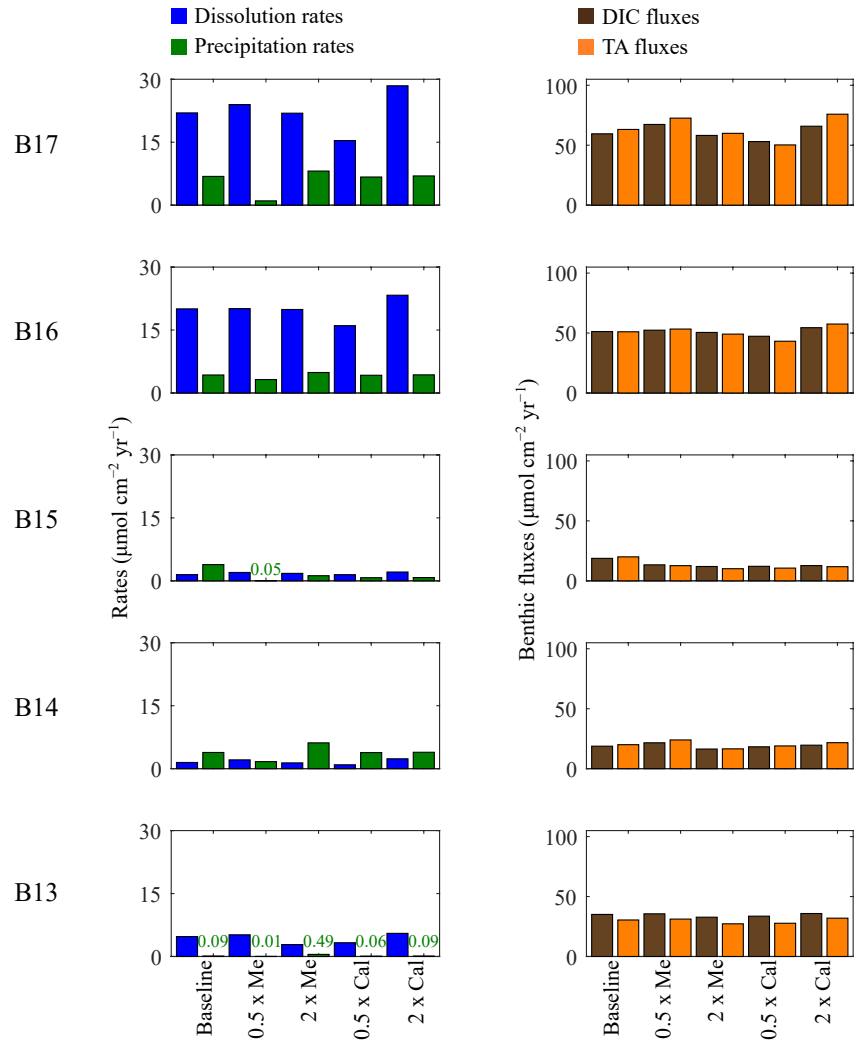

Figure 9. Sensitivity of seafloor carbonate chemistry parameters to changes in metal (oxyhydr)oxides (0.5x and 2x) and calcite (0.5x and 2x) export relative to baseline conditions (see main text). Left column: rates of dissolution (blue) and precipitation (green). Right column: Benthic fluxes of dissolution of inorganic carbon (DIC) (brown) and total alkalinity (TA) (orange).

these increases differ along the transect. At B13–B15, precipitation rates increase 2–3-fold relative to baseline conditions, whereas at B16–B17 rates are 4–5-fold higher (Table S3–S7 in Supporting Information S1). This regional difference may be attributed the high rates of OM degradation and greater contribution of metal oxide pathways in the northern sites relative to the southern area (Freitas et al., 2020). Furthermore, higher sedimentation rates would increase input fluxes of reactive OM, and thus lead to a shift from oxic to anoxic degradation pathways (Middelburg, 2019). Indeed, results show that higher sedimentation rates trigger a shift in metabolic pathways of OM degradation, such that the relative contribution of aerobic OM degradation decreases. This decrease is compensated by increases in metal oxide and OSR contributions, which particularly at B15–B17 leads to an increase in Ω. Consequently, rates of calcite dissolution slightly decrease due to pH buffering, while rates of precipitation significantly increase. Except for B13, these changes do not translate into important changes in $J_{DIC,Total}$ and $J_{TA,Total}$. At B13, fluxes increase due to enhanced DIC and TA production by OM degradation and further TA production by sulfide oxidation, which are not offset by limited authigenic carbonate precipitation (for details see Table S3 in Supporting Information S1).

Benthic OM degradation is donor controlled (Burdige, 2006) and rates of OM degradation in the Barents Sea scale with OM input at the SWI (März et al., 2022). Our results show that changes in OM input exert an important

influence on carbonate precipitation, and to a lesser extent on dissolution rates (Figure 8). Calcite dissolution rates slightly increase with lower OM deposition at the northern sites due to a shift in metabolic pathways. An OM content that is half of baseline conditions increases the relative contribution of aerobic OM degradation from 52% to 74% (Freitas et al., 2020) to 68%–88% (März et al., 2022). Under such conditions, there is deepening of the oxic layer into the sediments, which generally results in sustained low pH values (Forja et al., 2004; Jourabchi et al., 2005; Mucci et al., 2000; Soetaert et al., 2007). Moreover, reducing the OM input to half of its baseline values decreases TA production (Table S3–S7 in Supporting Information S1), and negatively affects precipitation rates. Since aerobic conditions prevail in these scenarios, metal oxide pathways are inhibited.

Conversely, doubling OM input leads to a 2–5-fold increase in carbonate precipitation rates at sites B14, B16, and B17 relative to baseline conditions. Under baseline conditions, these sites reveal the greatest metal oxide contributions to OM degradation (3%–11%; Freitas et al., 2020). The 2-fold increase in OM input results in an overall shift from aerobic to anaerobic OM degradation, where metal oxide contributions in B14, B16, and B17 make up 21%–35% of OM degradation rates (März et al., 2022). Here, metal oxide pathways promote a shallow pH increase and Ω oversaturation (Berner et al., 1970; Canfield et al., 1993; Green & Aller, 2001; Hu & Cai, 2011; Kostka et al., 1999; Tessin et al., 2020). Thus, concomitantly with an enhanced production of TA, these processes promote Ω oversaturation, leading to greater carbonate precipitation rates (Figure 8; Tables S3–S7 in Supporting Information S1). As a result of greater OM degradation rates under double OM input, we quantify an increase in DIC production. As such, benthic DIC fluxes also generally increase despite the DIC sink by authigenic precipitation (Tables S3–S7 in Supporting Information S1).

Mn and Fe (oxyhydr)oxides are relatively abundant in Barents Sea sediments (Faust et al., 2021; Kostka et al., 1999; Michaud et al., 2020; Nickel et al., 2008; Vandieken et al., 2006). The relative contributions of these metal oxides to OM degradation exert an important control on pH and carbonate chemistry of porewaters (Berner et al., 1970; Canfield et al., 1993; Green & Aller, 2001; Hu & Cai, 2011; Kostka et al., 1999; Tessin et al., 2020). Yet, our sensitivity tests show that changes in metal oxide inputs to the seafloor exert relatively minor impacts on carbonate dynamics in the Barents Sea (Figure 9; Table S3–S7 in Supporting Information S1). This somewhat counterintuitive result can be explained by the fact that depth-integrated carbonate dissolution and precipitation is mainly controlled by the residence time of the sediment layer within the carbonate dissolution and/or precipitation zone (Blouet et al., 2021). As a consequence, the redox zonation of the sediment exerts, next to the sedimentation rate, a first-order control on total carbonate dissolution and precipitation. Model results reveal that, in contrast to changes in OM inputs, changes in metal oxide input increase have a limited influence on the redox zonation of the sediment, and thus on the location and extent of the precipitation ($\Omega > 5$) and dissolution ($\Omega < 1$) zones.

Changes on calcite input fluxes alone to the seafloor are limited to relatively small shifts in dissolution rates. Unsurprisingly, an increase (decrease) in calcite inputs marginally triggers an increase (decrease) in dissolution rates (Figure 9; Table S3–S7 in Supporting Information S1). These impacts are more pronounced at B16–B17, and there are two likely explanations for this pattern. First, sites B16 and B17 are characterized by more corrosive pH conditions (pH < 7.45) and strong Ω undersaturation ($\Omega = 0.48$–0.68) in the upper 2 cm sediments, which is further sustained by intense proton production via aerobic OM degradation (Sections 3.1 and 3.2). In addition, these sites are more susceptible to bottom water acidification and Ω undersaturation (Section 3.4.1). Such conditions favor calcite dissolution, which is limited by the availability of calcite itself. Second, since calcite contents in the northern sites are higher than those found in B13–B15 (Table 1; Faust et al., 2020), any relative change in calcite input fluxes will have a much larger absolute impact on sites B16 and B17. Yet, those impacts are minimal when compared to more dominant factors, such changes in OM inputs (see above; Tables S3–S7 in Supporting Information S1).

3.5. Implications for a Changing Arctic Ocean

Our baseline assessment allowed us to identify the main drivers of seafloor pH and carbonate dynamics in the Barents Sea shelf, while our sensitivity tests illustrate how potential changes in these environmental conditions might affect DIC and TA fluxes in the Barents Sea. Although our analyses are focused on the Barents Sea shelf region, we showed systematic links between plausible environmental changes associated to sea-ice loss, Atlantification, and OA (Årthun et al., 2012; Barton et al., 2018; Oziel et al., 2020; Smedsrud et al., 2013). We provide a range of expected responses of seafloor inorganic carbon dynamics, which are critical because of the

ongoing changes experienced by the Barents Sea and are projected to affect the Arctic Ocean in its entirety (Lewis et al., 2020; Luo et al., 2016; Terhaar et al., 2019; 2020; Zhang et al., 2020).

The projected shoaling of carbonate compensation depths triggered by acidification of the Arctic Ocean will result in marked increase in shallow carbonate dissolution (Luo et al., 2016), and thus negatively impact PIC export to the seafloor. With the acidification of bottom waters, benthic calcite dissolution may become intensified and result in greater benthic fluxes of DIC and TA (Gazeau et al., 2014). However, these processes will be sustained at the expenses of PIC burial (Hulth et al., 1994; Steinsund & Hald, 1994), which can lead to a collapse of pH buffering by calcite dissolution. In contrast, changes in pelagic productivity by Atlantification and/or sea-ice loss (Lewis et al., 2020; Oziel et al., 2020) may shift OM export to the seafloor. As such, sediments may experience a shift in redox zonation (März et al., 2022), and inorganic carbon dynamics within sediments. Critically, enhanced input of OM to the seafloor could offset the impacts of bottom water acidification, although such increase in pelagic export would probably be accompanied by additional changes in environmental conditions, such as pelagic nutrient dynamics and changes in phytoplankton communities with further implications for benthic carbonate cycling (Lewis et al., 2020; Oziel et al., 2020).

Mechanistically understanding how these processes will critically tip the delicate balance of pH and carbonate dynamics in Arctic Ocean sediments is crucial. The Arctic Ocean is rapidly changing and will continue to do so (Huntington et al., 2022; Khosravi et al., 2022; März et al., 2022; Thomas et al., 2022; Tuerena et al., 2022). Here, we offer some systematic insights that can help in building a comprehensive picture for the entire Barents Sea shelf and foster further investigations to interrogate other biogeochemical drivers. Our study can help to develop an informed Pan-Arctic picture of processes governing pH and Ω, as well as carbonate burial and feedbacks to bottom waters for the near future (e.g., end of century), which would complement currently available pelagic assessments (Bindoff et al., 2019; Khosravi et al., 2022; Luo et al., 2016; Meredith et al., 2019; Terhaar et al., 2019; 2020).

4. Conclusions

Using a model-data approach calibrated for OM dynamics in the Barents Sea shelf (Freitas et al., 2020), we explicitly resolved benthic pH and carbonate systems and quantified the diagenetic processes governing shifts in porewater pH and saturation state, as well as DIC and TA fluxes. Further, we assessed how bottom water conditions and input fluxes impact inorganic carbon dynamics and its links to environmental changes.

1. Our assessments are in general agreement with findings that OM transformation plays an important role for pH and Ω. Further, we also show the important role played by bottom water conditions in shaping pH and Ω saturation close to the sediment-water interface. Importantly, here we systematically quantified the interconnected role of these processes and their impacts on pH buffering capacity, as well as calcite dissolution and precipitation.
2. We identified a marked South—North pattern along the Barents Sea 30°E transect, which somewhat coincides with the prevailing water mass and sea ice gradients. The S—N pattern controls the depth evolutions and intensities of pH negative shift and Ω undersaturation ($\Omega < 1$) driven by bottom waters carbonate chemistry alongside aerobic OM degradation in the upper 2–5 cm depth. These processes drive calcite dissolution, as well as pH increase and Ω oversaturation ($\Omega > 5$) produced by metal oxide pathways deeper than 5–10 cm that enables calcite authigenic precipitation.
3. We calculated benthic DIC and TA fluxes, which are 2–3-fold greater in the northern sites. In the southern sites (B13–B15), DIC and TA fluxes are mainly driven by OM degradation. In contrast, greater fluxes in the northern sites (B16–B17) are produced by both OM degradation and strong calcite dissolution, the latter due to greater $CaCO_3$ availability and shallow Ω undersaturation.
4. The Barents Sea sediments are vulnerable to bottom waters acidification, particularly in the northern, calcite-rich sites. We showed that a drop in pH relative to present-day conditions can produce large dissolution, which is expressed by intensified DIC and TA fluxes. In contrast, intensification of OM export fluxes to the seafloor may lead to a shift in redox conditions and promote an intensification of metal oxide pathways. This can strengthen Ω oversaturation and counter the effects of bottom waters acidification.

Our work opens doors for future analyses aiming to critically explore the sensitivity of the Arctic Ocean seafloor toward the complex, yet uncertain impacts of Atlantification, sea ice loss, and ocean acidification. This can lead to a mechanistic understanding and forecasting of pH and carbonate dynamics for the end of the 21st century.

Conflict of Interest

The authors declare no conflicts of interest relevant to this study.

Data Availability Statement

The model employed here is based on Freitas et al. (2020). The updated model code with the implemented pH and carbonate dynamics is available at the Zonedo repository (Freitas, 2022; https://doi.org/10.5281/zenodo.6384988).

Acknowledgments
We thank the crew and participants of cruises JR16006 and JR17007, RRS *James Clark Ross*, and logistic support from the National Marine Facilities (NMF, Southampton, UK), and the British Antarctic Survey (BAS, Cambridge, UK). This work is part of the Changing Arctic Ocean Seafloor (ChAOS) project, funded by the UKRI-NERC (grant NE/P006493/1 and NE/P005942-1). Computational resources have been provided by the Consortium des Équipements de Calcul Intensif (CÉCI), funded by the Fonds de la Recherche Scientifique de Belgique (F.R.S.-FNRS) under Grant No. 2.5020.11 and by the Walloon Region, Belgium. AT received funding from the European Union's Horizon 2020 research and innovation programme under the Marie Skłodowska-Curie grant agreement No 709175.

References

Adler, M., Hensen, C., Wenzhöfer, F., Pfeifer, K., & Schulz, H. D. (2001). Modeling of calcite dissolution by oxic respiration in supralysoclinal deep-sea sediments. *Marine Geology*, *177*(1), 167–189. https://doi.org/10.1016/S0025-3227(01)00130-X

Aguilera, D. R., Jourabchi, P., Spiteri, C., & Regnier, P. (2005). A knowledge-based reactive transport approach for the simulation of biogeochemical dynamics in Earth systems. *Geochemistry, Geophysics, Geosystems*, *6*(7). https://doi.org/10.1029/2004GC000899

Årthun, M., Eldevik, T., Smedsrud, L. H., Skagseth, Ø., & Ingvaldsen, R. B. (2012). Quantifying the influence of Atlantic heat on Barents Sea ice variability and retreat. *Journal of Climate*, *25*(13), 4736–4743. https://doi.org/10.1175/JCLI-D-11-00466.1

Barton, B. I., Lenn, Y.-D., & Lique, C. (2018). Observed Atlantification of the Barents Sea causes the polar front to limit the expansion of winter sea ice. *Journal of Physical Oceanography*, *48*(8), 1849–1866. https://doi.org/10.1175/JPO-D-18-0003.1

Bates, N. R., & Mathis, J. T. (2009). The Arctic Ocean marine carbon cycle: Evaluation of air-sea CO_2 exchanges, ocean acidification impacts and potential feedbacks. *Biogeosciences*, *6*(11), 2433–2459. https://doi.org/10.5194/bg-6-2433-2009

Ben-Yaakov, S. (1973). pH buffering of pore water of recent anoxic marine sediments. *Limnology & Oceanography*, *18*(1), 86–94. https://doi.org/10.4319/lo.1973.18.1.0086

Berelson, W. M., Hammond, D. E., & Cutter, G. A. (1990). In situ measurements of calcium carbonate dissolution rates in deep-sea sediments. *Geochimica et Cosmochimica Acta*, *54*(11), 3013–3020. https://doi.org/10.1016/0016-7037(90)90118-5

Berelson, W. M., Hammond, D. E., & Johnson, K. S. (1987). Benthic fluxes and the cycling of biogenic silica and carbon in two southern California borderland basins. *Geochimica et Cosmochimica Acta*, *51*(6), 1345–1363. https://doi.org/10.1016/0016-7037(87)90320-6

Berelson, W. M., Hammond, D. E., McManus, J., & Kilgore, T. E. (1994). Dissolution kinetics of calcium carbonate in equatorial Pacific sediments. *Global Biogeochemical Cycles*, *8*(2), 219–235. https://doi.org/10.1029/93GB03394

Berelson, W. M., McManus, J., Coale, K., Johnson, K., Burdige, D., Kilgore, T., et al. (2003). A time series of benthic flux measurements from Monterey Bay, CA. *Continental Shelf Research*, *23*(5), 457–481. https://doi.org/10.1016/S0278-4343(03)00009-8

Berelson, W. M., McManus, J., Severmann, S., & Rollins, N. (2019). Benthic fluxes from hypoxia-influenced Gulf of Mexico sediments: Impact on bottom water acidification. *Marine Chemistry*, *209*, 94–106. https://doi.org/10.1016/j.marchem.2019.01.004

Berner, R. A., Scott, M. R., & Thomlinson, C. (1970). Carbonate alkalinity in the porewaters of anoxic marine sediments. *Limnology & Oceanography*, *15*(4), 544–549. https://doi.org/10.4319/lo.1970.15.4.0544

Bindoff, N. L., Cheung, W. W. L., Kairo, J. G., Arístegui, J., Guinder, V. A., Hallberg, R., et al. (2019). Changing ocean, marine ecosystems, and dependent communities. In H.-O. Pörtner, D. C. Roberts, V. Masson-Delmotte, P. Zhai, M. Tignor, E. Poloczanska, et al. (Eds.), *IPCC special report on the ocean and cryosphere in a changing climate*. Retrieved from https://www.ipcc.ch/srocc/chapter/chapter-5/

Blouet, J.-P., Arndt, S., Imbert, P., & Regnier, P. (2021). Are seep carbonates quantitative proxies of CH_4 leakage? Modeling the influence of sulfate reduction and anaerobic oxidation of methane on pH and carbonate precipitation. *Chemical Geology*, *577*, 120254. https://doi.org/10.1016/j.chemgeo.2021.120254

Bourgeois, S., Archambault, P., & Witte, U. (2017). Organic matter remineralization in marine sediments: A pan-Arctic synthesis. *Global Biogeochemical Cycles*, *31*(1), 190–213. https://doi.org/10.1002/2016GB005378

Burdige, D. J. (2006). *Geochemistry of marine sediments*. Princeton University Press.

Cai, W.-J., Chen, L., Chen, B., Gao, Z., Lee, S. H., Chen, J., et al. (2010). Decrease in the CO_2 uptake capacity in an ice-free Arctic Ocean basin. *Science*, *329*(5991), 556. https://doi.org/10.1126/science.1189338

Cai, W.-J., & Reimers, C. E. (1993). The development of pH and pCO_2 microelectrodes for studying the carbonate chemistry of pore waters near the sediment-water interface. *Limnology & Oceanography*, *38*(8), 1762–1773. https://doi.org/10.4319/lo.1993.38.8.1762

Cai, W.-J., Zhao, P., & Wang, Y. (2000). pH and pCO_2 microelectrode measurements and the diffusive behavior of carbon dioxide species in coastal marine sediments. *Marine Chemistry*, *70*(1), 133–148. https://doi.org/10.1016/S0304-4203(00)00017-7

Canfield, D. E., Jørgensen, B. B., Fossing, H., Glud, R., Gundersen, J., Ramsing, N. B., et al. (1993). Pathways of organic carbon oxidation in three continental margin sediments. *Marine Geology*, *113*(1), 27–40. https://doi.org/10.1016/0025-3227(93)90147-N

Carmack, E., & Wassmann, P. (2006). Food webs and physical–biological coupling on pan-Arctic shelves: Unifying concepts and comprehensive perspectives. *Progress in Oceanography*, *71*(2), 446–477. https://doi.org/10.1016/j.pocean.2006.10.004

Chen, C.-T. A., & Borges, A. V. (2009). Reconciling opposing views on carbon cycling in the coastal ocean: Continental shelves as sinks and near-shore ecosystems as sources of atmospheric CO_2. *Surface Ocean CO2 Variability and Vulnerabilities*, *56*(8), 578–590. https://doi.org/10.1016/j.dsr2.2009.01.001

Cochrane, S. K. J., Denisenko, S. G., Renaud, P. E., Emblow, C. S., Ambrose, W. G., Ellingsen, I. H., & Skarðhamar, J. (2009). Benthic macrofauna and productivity regimes in the Barents Sea—Ecological implications in a changing Arctic. *Journal of Sea Research*, *61*(4), 222–233. https://doi.org/10.1016/j.seares.2009.01.003

Dalpadado, P., Arrigo, K. R., van Dijken, G. L., Skjoldal, H. R., Bagøien, E., Dolgov, A. V., et al. (2020). Climate effects on temporal and spatial dynamics of phytoplankton and zooplankton in the Barents Sea. *Progress in Oceanography*, *185*, 102320. https://doi.org/10.1016/j.pocean.2020.102320

Demina, L. L., Dara, O., Aliev, R., Alekseeva, T., Budko, D., Novichkova, E., et al. (2020). Elemental and mineral composition of the Barents Sea recent and late Pleistocene−Holocene sediments: A correlation with environmental conditions. *Minerals*, *10*(7), 593. https://doi.org/10.3390/min10070593

Dollar, S. J., Smith, S. V., Vink, S. M., Obrebski, S., & Hollibaugh, J. T. (1991). Annual cycle of benthic nutrient fluxes in Tomales Bay, California, and contribution of the benthos to total ecosystem metabolism. *Marine Ecology Progress Series*, *79*, 115–125. https://doi.org/10.3354/meps079115

Doney, S. C., Busch, D. S., Cooley, S. R., & Kroeker, K. J. (2020). The impacts of ocean acidification on marine ecosystems and reliant human communities. *Annual Review of Environment and Resources*, *45*(1), 83–112. https://doi.org/10.1146/annurev-environ-012320-083019

Downes, P. P., Goult, S. J., Woodward, E. M. S., Widdicombe, C. E., Tait, K., & Dixon, J. L. (2021). Phosphorus dynamics in the Barents Sea. *Limnology & Oceanography*, *66*(S1), S326–S342. https://doi.org/10.1002/lno.11602

Else, B. G. T., Galley, R. J., Lansard, B., Barber, D. G., Brown, K., Miller, L. A., et al. (2013). Further observations of a decreasing atmospheric CO_2 uptake capacity in the Canada Basin (Arctic Ocean) due to sea ice loss. *Geophysical Research Letters*, *40*(6), 1132–1137. https://doi.org/10.1002/grl.50268

Emerson, S. R., & Archer, D. (1990). Calcium carbonate preservation in the ocean. *Philosophical Transactions of the Royal Society of London—Series A: Mathematical and Physical Sciences*, *331*(1616), 29–40.

Fabry, V. J., Seibel, B. A., Feely, R. A., & Orr, J. C. (2008). Impacts of ocean acidification on marine fauna and ecosystem processes. *ICES Journal of Marine Science*, *65*(3), 414–432. https://doi.org/10.1093/icesjms/fsn048

Faust, J. C., Stevenson, M. A., Abbott, G. D., Knies, J., Tessin, A., Mannion, I., et al. (2020). Does Arctic warming reduce preservation of organic matter in Barents Sea sediments? *Philosophical Transactions of the Royal Society A: Mathematical, Physical & Engineering Sciences*, *378*(2181), 20190364. https://doi.org/10.1098/rsta.2019.0364

Faust, J. C., Tessin, A., Fisher, B. J., Zindorf, M., Papadaki, S., Hendry, K. R., et al. (2021). Millennial scale persistence of organic carbon bound to iron in Arctic marine sediments. *Nature Communications*, *12*(1), 275. https://doi.org/10.1038/s41467-020-20550-0

Forja, J. M., Ortega, T., DelValls, T. A., & Gómez-Parra, A. (2004). Benthic fluxes of inorganic carbon in shallow coastal ecosystems of the Iberian Peninsula. *Marine Chemistry*, *85*(3), 141–156. https://doi.org/10.1016/j.marchem.2003.09.007

Freitas, F. S. (2022). Model code: Benthic organic matter transformation drives pH and carbonate chemistry in Arctic marine sediments (Barents-Sea_BRNS_pH_carbonates) [Computer software]. Zenodo, https://doi.org/10.5281/ZENODO.6384988

Freitas, F. S., Hendry, K. R., Henley, S. F., Faust, J. C., Tessin, A. C., Stevenson, M. A., et al. (2020). Benthic-pelagic coupling in the Barents Sea: An integrated data-model framework. *Philosophical Transactions of the Royal Society A: Mathematical, Physical & Engineering Sciences*, *378*(2181), 20190359. https://doi.org/10.1098/rsta.2019.0359

Freitas, F. S., Pika, P. A., Kasten, S., Jørgensen, B. B., Rassmann, J., Rabouille, C., et al. (2021). New insights into large-scale trends of apparent organic matter reactivity in marine sediments and patterns of benthic carbon transformation. *Biogeosciences*, *18*(15), 4651–4679. https://doi.org/10.5194/bg-18-4651-2021

Friedlingstein, P., Jones, M. W., O'Sullivan, M., Andrew, R. M., Hauck, J., Peters, G. P., et al. (2019). Global carbon budget 2019. *Earth System Science Data*, *11*(4), 1783–1838. https://doi.org/10.5194/essd-11-1783-2019

Gattuso, J.-P., & Hansson, L. (Eds.) (2011). *Ocean acidification*. Oxford University Press.

Gazeau, F., van Rijswijk, P., Pozzato, L., & Middelburg, J. J. (2014). Impacts of ocean acidification on sediment processes in shallow waters of the Arctic Ocean. *PLoS ONE*, *9*(4), e94068. https://doi.org/10.1371/journal.pone.0094068

Green, M. A., & Aller, R. C. (2001). Early diagenesis of calcium carbonate in Long Island Sound sediments: Benthic fluxes of Ca^{2+} and minor elements during seasonal periods of net dissolution. *Journal of Marine Research*, *59*(5), 769–794. https://doi.org/10.1357/002224001762674935

Guinotte, J. M., & Fabry, V. J. (2008). Ocean acidification and its potential effects on marine ecosystems. *Annals of the New York Academy of Sciences*, *1134*(1), 320–342. https://doi.org/10.1196/annals.1439.013

Hales, B., Emerson, S., & Archer, D. (1994). Respiration and dissolution in the sediments of the western North Atlantic: Estimates from models of in situ microelectrode measurements of porewater oxygen and pH. *Deep Sea Research Part I: Oceanographic Research Papers*, *41*(4), 695–719. https://doi.org/10.1016/0967-0637(94)90050-7

Hammond, D. E., McManus, J., Berelson, W. M., Kilgore, T. E., & Pope, R. H. (1996). Early diagenesis of organic material in equatorial Pacific sediments: Stoichiometry and kinetics. *Deep Sea Research Part II: Topical Studies in Oceanography*, *43*(4), 1365–1412. https://doi.org/10.1016/0967-0645(96)00027-6

Henley, S. F., Porter, M., Hobbs, L., Braun, J., Guillaume-Castel, R., Venables, E. J., et al. (2020). Nitrate supply and uptake in the Atlantic Arctic sea ice zone: Seasonal cycle, mechanisms and drivers. *Philosophical Transactions of the Royal Society A: Mathematical, Physical & Engineering Sciences*, *378*(2181), 20190361. https://doi.org/10.1098/rsta.2019.0361

Hu, X., & Cai, W.-J. (2011). An assessment of ocean margin anaerobic processes on oceanic alkalinity budget. *Global Biogeochemical Cycles*, *25*(3). https://doi.org/10.1029/2010GB003859

Hulth, S., Blackburn, T. H., & Hall, P. O. J. (1994). Arctic sediments (Svalbard): Consumption and microdistribution of oxygen. *Marine Chemistry*, *46*(3), 293–316. https://doi.org/10.1016/0304-4203(94)90084-1

Hulth, S., Hall, P. O. J., Landén, A., & Blackburn, T. H. (1996). Arctic sediments (Svalbard): Pore water and solid phase distributions of C, N, P and Si. *Polar Biology*, *16*(6), 447–462. https://doi.org/10.1007/BF02390426

Huntington, H. P., Zagorsky, A., Kaltenborn, B. P., Shin, H. C., Dawson, J., Lukin, M., et al. (2022). Societal implications of a changing Arctic Ocean. *Ambio*, *51*(2), 298–306. https://doi.org/10.1007/s13280-021-01601-2

Husum, K., Ninnemann, U., Rydningen, T. A., Alve, E., Altuna, N. E. B., Braaten, A. H., et al. (2020). Paleo cruise 2018. In *The Nansen Legacy Report Series* (Vol. *3*). https://doi.org/10.7557/nlrs.5502

Jahnke, R. A., Craven, D. B., & Gaillard, J.-F. (1994). The influence of organic matter diagenesis on $CaCO_3$ dissolution at the deep-sea floor. *Geochimica et Cosmochimica Acta*, *58*(13), 2799–2809. https://doi.org/10.1016/0016-7037(94)90115-5

Jahnke, R. A., Craven, D. B., McCorkle, D. C., & Reimers, C. E. (1997). $CaCO_3$ dissolution in California continental margin sediments: The influence of organic matter remineralization. *Geochimica et Cosmochimica Acta*, *61*(17), 3587–3604. https://doi.org/10.1016/S0016-7037(97)00184-1

Jahnke, R. A., Heggie, D., Emerson, S., & Grundmanis, V. (1982). Pore waters of the central Pacific Ocean: Nutrient results. *Earth and Planetary Science Letters*, *61*(2), 233–256. https://doi.org/10.1016/0012-821X(82)90056-5

Jahnke, R. A., & Jahnke, D. B. (2000). Rates of C, N, P and Si recycling and denitrification at the US Mid-Atlantic continental slope depocenter. *Deep Sea Research Part I: Oceanographic Research Papers*, *47*(8), 1405–1428. https://doi.org/10.1016/S0967-0637(99)00118-1

Jahnke, R. A., & Jahnke, D. B. (2004). Calcium carbonate dissolution in deep sea sediments: Reconciling microelectrode, pore water and benthic flux chamber results. *Geochimica et Cosmochimica Acta*, *68*(1), 47–59. https://doi.org/10.1016/S0016-7037(03)00260-6

Jahnke, R. A., Reimers, C. E., & Craven, D. B. (1990). Intensification of recycling of organic matter at the sea floor near ocean margins. *Nature*, *348*(6296), 50–54. https://doi.org/10.1038/348050a0

Jones, E., Chierici, M., Skjelvan, I., Norli, M., Børsheim, K. Y., Lødemel, H. H., et al. (2019). Monitoring ocean acidification in Norwegian seas in 2018. M–1417).

Jourabchi, P., Van Cappellen, P., & Regnier, P. (2005). Quantitative interpretation of pH distributions in aquatic sediments: A reaction-transport modeling approach. *American Journal of Science*, *305*(9), 919–956. https://doi.org/10.2475/ajs.305.9.919

Jutterström, S., & Anderson, L. G. (2005). The saturation of calcite and aragonite in the Arctic Ocean. *Marine Chemistry*, *94*(1), 101–110. https://doi.org/10.1016/j.marchem.2004.08.010

Kaltin, S., Anderson, L. G., Olsson, K., Fransson, A., & Chierici, M. (2002). Uptake of atmospheric carbon dioxide in the Barents Sea. *Seasonal C-Cycling Variability in the Open and Ice-Covered Waters of the Barents Sea*, *38*(1), 31–45. https://doi.org/10.1016/S0924-7963(02)00168-9

Khosravi, N., Wang, Q., Koldunov, N., Hinrichs, C., Semmler, T., Danilov, S., & Jung, T. (2022). The Arctic Ocean in CMIP6 models: Biases and projected changes in temperature and salinity. *Earth's Future*, *10*(2), e2021EF002282. https://doi.org/10.1029/2021EF002282

Knies, J., & Stein, R. (1998). New aspects of organic carbon deposition and its paleoceanographic implications along the Northern Barents Sea Margin during the last 30,000 years. *Paleoceanography*, *13*(4), 384–394. https://doi.org/10.1029/98PA01501

Kostka, J. E., Thamdrup, B., Glud, R. N., & Canfield, D. E. (1999). *Rates and pathways of carbon oxidation in permanently cold Arctic sediments*. In *Marine Ecology Progress Series* (Vol. 180, pp. 7–21). JSTOR. https://doi.org/10.3354/meps180007

Kroeker, K. J., Kordas, R. L., Crim, R. N., & Singh, G. G. (2010). Meta-analysis reveals negative yet variable effects of ocean acidification on marine organisms. *Ecology Letters*, *13*(11), 1419–1434. https://doi.org/10.1111/j.1461-0248.2010.01518.x

Krumins, V., Gehlen, M., Arndt, S., VanCappellen, P., & Regnier, P. (2013). Dissolved inorganic carbon and alkalinity fluxes from coastal marine sediments: Model estimates for different shelf environments and sensitivity to global change. *Biogeosciences*, *10*(1), 371–398. https://doi.org/10.5194/bg-10-371-2013

Lewis, K. M., van Dijken, G. L., & Arrigo, K. R. (2020). Changes in phytoplankton concentration now drive increased Arctic Ocean primary production. *Science*, *369*(6500), 198. https://doi.org/10.1126/science.aay8380

Luff, R., Haeckel, M., & Wallmann, K. (2001). Robust and fast FORTRAN and MATLAB® libraries to calculate pH distributions in marine systems. *Computers & Geosciences*, *27*(2), 157–169. https://doi.org/10.1016/S0098-3004(00)00097-2

Luo, Y., Boudreau, B. P., & Mucci, A. (2016). Disparate acidification and calcium carbonate desaturation of deep and shallow waters of the Arctic Ocean. *Nature Communications*, *7*(1), 12821. https://doi.org/10.1038/ncomms12821

Mackenzie, F. T., Vink, S., Wollast, R., & Chou, L. (1995). Comparative geochemistry of marine saline lakes. In A. Lerman, D. M. Imboden, & J. R. Gat (Eds.), *Physics and chemistry of lakes* (pp. 265–278). Springer Berlin Heidelberg. https://doi.org/10.1007/978-3-642-85132-2_9

Martens, J., Romankevich, E., Semiletov, I., Wild, B., van Dongen, B., Vonk, J., et al. (2021). CASCADE—The circum-Arctic sediment CArbon DatabasE. *Earth System Science Data*, *13*(6), 2561–2572. https://doi.org/10.5194/essd-13-2561-2021

März, C., Freitas, F. S., Faust, J. C., Godbold, J. A., Henley, S. F., Tessin, A. C., et al. (2022). Biogeochemical consequences of a changing Arctic shelf seafloor ecosystem. *Ambio*, *51*(2), 370–382. https://doi.org/10.1007/s13280-021-01638-3

Meredith, M., Sommerkorn, M., Cassotta, S., Derksen, C., Ekaykin, A., Hollowed, A., et al. (2019). Polar regions. In H.-O. Pörtner, D. C. Roberts, V. Masson-Delmotte, P. Zhai, M. Tignor, E. Poloczanska, et al. (Eds.), *IPCC special report on the ocean and cryosphere in a changing climate*. Retrieved from https://www.ipcc.ch/srocc/chapter/chapter-3-2/

Michaud, A. B., Laufer, K., Findlay, A., Pellerin, A., Antler, G., Turchyn, A. V., et al. (2020). Glacial influence on the iron and sulfur cycles in Arctic fjord sediments (Svalbard). *Geochimica et Cosmochimica Acta*, *280*, 423–440. https://doi.org/10.1016/j.gca.2019.12.033

Middelburg, J. J. (2019). *Marine carbon Biogeochemistry: A primer for Earth system scientists* (1st edn). Springer International Publishing: Imprint: Springer. https://doi.org/10.1007/978-3-030-10822-9

Middelburg, J. J., Soetaert, K., & Hagens, M. (2020). Ocean alkalinity, buffering and biogeochemical processes. *Reviews of Geophysics*, *58*(3), e2019RG000681. https://doi.org/10.1029/2019RG000681

Miller, C. M., Dickens, G. R., Jakobsson, M., Johansson, C., Koshurnikov, A., O'Regan, M., et al. (2017). Pore water geochemistry along continental slopes north of the East Siberian Sea: Inference of low methane concentrations. *Biogeosciences*, *14*(12), 2929–2953. https://doi.org/10.5194/bg-14-2929-2017

Millero, F. J. (1995). Thermodynamics of the carbon dioxide system in the oceans. *Geochimica et Cosmochimica Acta*, *59*(4), 661–677. https://doi.org/10.1016/0016-7037(94)00354-O

Millero, F. J. (2000). The carbonate system in marine environments. In A. Gianguzza, E. Pelizetti, & S. Sammartano (Eds.), *Chemical processes in marine environments* (pp. 9–41). Springer Berlin Heidelberg. https://doi.org/10.1007/978-3-662-04207-6_2

Morata, N., & Renaud, P. E. (2008). Sedimentary pigments in the western Barents Sea: A reflection of pelagic–benthic coupling? *Deep Sea Research Part II: Topical Studies in Oceanography*, *55*(20), 2381–2389. https://doi.org/10.1016/j.dsr2.2008.05.004

Morse, J. W. (1983). *The kinetics of calcium carbonate dissolution and precipitation* In R. J. Reeder (Ed.), pp. *227–264*). De Gruyter. https://doi.org/10.1515/9781501508134-011

Morse, J. W., & Beazley, M. J. (2008). Organic matter in deepwater sediments of the northern Gulf of Mexico and its relationship to the distribution of benthic organisms. *Deep Sea Research Part II: Topical Studies in Oceanography*, *55*(24), 2563–2571. https://doi.org/10.1016/j.dsr2.2008.07.004

Morse, J. W., Gledhill, D. K., & Millero, F. J. (2003). $CaCO_3$ precipitation kinetics in waters from the great Bahama bank. *Geochimica et Cosmochimica Acta*, *67*(15), 2819–2826. https://doi.org/10.1016/S0016-7037(03)00103-0

Morse, J. W., & Mackenzie, F. T. (1990). *Geochemistry of sedimentary carbonates*. Elsevier; Distributors for the U.S. and Canada, Elsevier Science Pub. Co.

Mucci, A., Sundby, B., Gehlen, M., Arakaki, T., Zhong, S., & Silverberg, N. (2000). The fate of carbon in continental shelf sediments of eastern Canada: A case study. *Deep Sea Research Part II: Topical Studies in Oceanography*, *47*(3), 733–760. https://doi.org/10.1016/S0967-0645(99)00124-1

Nickel, M., Vandieken, V., Brüchert, V., & Jørgensen, B. B. (2008). Microbial Mn(IV) and Fe(III) reduction in northern Barents Sea sediments under different conditions of ice cover and organic carbon deposition. *Deep Sea Research Part II: Topical Studies in Oceanography*, *55*(20), 2390–2398. https://doi.org/10.1016/j.dsr2.2008.05.003

Ortega, T., Ponce, R., Forja, J., & Gómez-Parra, A. (2008). Benthic fluxes of dissolved inorganic carbon in the Tinto–Odiel system (SW of Spain). *Continental Shelf Research*, *28*(3), 458–469. https://doi.org/10.1016/j.csr.2007.10.004

Oziel, L., Baudena, A., Ardyna, M., Massicotte, P., Randelhoff, A., Sallée, J.-B., et al. (2020). Faster Atlantic currents drive poleward expansion of temperate phytoplankton in the Arctic Ocean. *Nature Communications*, *11*(1), 1705. https://doi.org/10.1038/s41467-020-15485-5

Oziel, L., Sirven, J., & Gascard, J.-C. (2016). The Barents Sea frontal zones and water masses variability (1980–2011). *Ocean Science*, *12*(1), 169–184. https://doi.org/10.5194/os-12-169-2016

Pautova, L. A., Silkin, V. A., Kravchishina, M. D., Chultsova, A. L., & Lisitzin, A. P. (2020). The biological calcium carbonate pump in the Norwegian and Barents Seas: Regulation Mechanisms. *Doklady Earth Sciences*, *490*(1), 46–50. https://doi.org/10.1134/S1028334X20010079

Rassmann, J., Eitel, E. M., Lansard, B., Cathalot, C., Brandily, C., Taillefert, M., & Rabouille, C. (2020). Benthic alkalinity and dissolved inorganic carbon fluxes in the Rhône River prodelta generated by decoupled aerobic and anaerobic processes. *Biogeosciences*, *17*(1), 13–33. https://doi.org/10.5194/bg-17-13-2020

Regnier, P., O'Kane, J. P., Steefel, C. I., & Vanderborght, J. P. (2002). Modeling complex multi-component reactive-transport systems: Towards a simulation environment based on the concept of a Knowledge Base. *Applied Mathematical Modelling*, *26*(9), 913–927. https://doi.org/10.1016/S0307-904X(02)00047-1

Reigstad, M., Wexels Riser, C., Wassmann, P., & Ratkova, T. (2008). Vertical export of particulate organic carbon: Attenuation, composition and loss rates in the northern Barents Sea. *Deep Sea Research Part II: Topical Studies in Oceanography*, *55*(20), 2308–2319. https://doi.org/10.1016/j.dsr2.2008.05.007

Ruttenberg, K. C. (2014). 10.13—The global phosphorus cycle. In H. D. Holland, & K. K. Turekian (Eds.), *Treatise on geochemistry* (2nd edn, pp. 499–558). Elsevier. https://doi.org/10.1016/B978-0-08-095975-7.00813-5

Schlitzer, R. (2021). Ocean Data View. odv.awi.de.

Semiletov, I., Pipko, I., Gustafsson, Ö., Anderson, L. G., Sergienko, V., Pugach, S., et al. (2016). Acidification of East Siberian Arctic Shelf waters through addition of freshwater and terrestrial carbon. *Nature Geoscience*, *9*(5), 361–365. https://doi.org/10.1038/ngeo2695

Slomp, C. P., Epping, E. H. G., Helder, W., & Raaphorst, W. V. (1996). A key role for iron-bound phosphorus in authigenic apatite formation in North Atlantic continental platform sediments. *Journal of Marine Research*, *54*(6), 1179–1205. https://doi.org/10.1357/0022240963213745

Smedsrud, L. H., Esau, I., Ingvaldsen, R. B., Eldevik, T., Haugan, P. M., Li, C., et al. (2013). The role of the Barents Sea in the Arctic climate system. *Reviews of Geophysics*, *51*(3), 415–449. https://doi.org/10.1002/rog.20017

Smith, S. V., Wiebe, W. J., Hollibaugh, J. T., Dollar, S. J., Hager, S. W., Cole, B. E., et al. (1987). Stoichiometry of C, N, P, and Si fluxes in a temperate-climate embayment. *Journal of Marine Research*, *45*(2), 427–460. https://doi.org/10.1357/002224087788401124

Soetaert, K., Hofmann, A. F., Middelburg, J. J., Meysman, F. J. R., & Greenwood, J. (2007). The effect of biogeochemical processes on pH. *Marine Chemistry*, *105*(1), 30–51. https://doi.org/10.1016/j.marchem.2006.12.012

Solan, M., Ward, E. R., Wood, C. L., Reed, A. J., Grange, L. J., & Godbold, J. A. (2020). Climate-driven benthic invertebrate activity and biogeochemical functioning across the Barents Sea polar front. *Philosophical Transactions of the Royal Society A: Mathematical, Physical & Engineering Sciences*, *378*(2181), 20190365. https://doi.org/10.1098/rsta.2019.0365

Solheim, A., & Elverhoi, A. (1996). Surface sediments of the north-western Barents Sea. In R. Stein, G. I. Ivanov, M. A. Levitan, & K. Fahl (Eds.), *Surface-sediment composition and sedimentary processes in the central Arctic Ocean and along the Eurasian continental margin*.

Souster, T. A., Barnes, D. K. A., & Hopkins, J. (2020). Variation in zoobenthic blue carbon in the Arctic's Barents Sea shelf sediments. *Philosophical Transactions of the Royal Society A: Mathematical, Physical & Engineering Sciences*, *378*(2181), 20190362. https://doi.org/10.1098/rsta.2019.0362

Steinsund, P. I., & Hald, M. (1994). Recent calcium carbonate dissolution in the Barents Sea: Paleoceanographic applications. *Marine Geology*, *117*(1), 303–316. https://doi.org/10.1016/0025-3227(94)90022-1

Stevenson, M. A., & Abbott, G. D. (2019). Exploring the composition of macromolecular organic matter in Arctic Ocean sediments under a changing sea ice gradient. *Journal of Analytical and Applied Pyrolysis*, *140*, 102–111. https://doi.org/10.1016/j.jaap.2019.02.006

Stevenson, M. A., Faust, J. C., Andrade, L. L., Freitas, F. S., Gray, N. D., Tait, K., et al. (2020). Transformation of organic matter in a Barents Sea sediment profile: Coupled geochemical and microbiological processes. *Philosophical Transactions of the Royal Society A: Mathematical, Physical & Engineering Sciences*, *378*(2181), 20200223. https://doi.org/10.1098/rsta.2020.0223

Terhaar, J., Kwiatkowski, L., & Bopp, L. (2020). Emergent constraint on Arctic Ocean acidification in the twenty-first century. *Nature*, *582*(7812), 379–383. https://doi.org/10.1038/s41586-020-2360-3

Terhaar, J., Orr, J. C., Gehlen, M., Ethé, C., & Bopp, L. (2019). Model constraints on the anthropogenic carbon budget of the Arctic Ocean. *Biogeosciences*, *16*(11), 2343–2367. https://doi.org/10.5194/bg-16-2343-2019

Tessin, A., März, C., Blais, M.-A., Brumsack, H.-J., Matthiessen, J., O'Regan, M., & Schnetger, B. (2020). Arctic continental margin sediments as possible Fe and Mn sources to seawater as sea ice retreats: Insights from the Eurasian Margin. *Global Biogeochemical Cycles*, *34*(8), e2020GB006581. https://doi.org/10.1029/2020GB006581

Thomas, D. N., Arévalo-Martínez, D. L., Crocket, K. C., Große, F., Grosse, J., Schulz, K., et al. (2022). A changing Arctic Ocean. *Ambio*, *51*(2), 293–297. https://doi.org/10.1007/s13280-021-01677-w

Thullner, M., Dale, A. W., & Regnier, P. (2009). Global-scale quantification of mineralization pathways in marine sediments: A reaction-transport modeling approach. *Geochemistry, Geophysics, Geosystems*, *10*(10). https://doi.org/10.1029/2009GC002484

Tuerena, R. E., Hopkins, J., Ganeshram, R. S., Norman, L., de la Vega, C., Jeffreys, R., & Mahaffey, C. (2021). Nitrate assimilation and regeneration in the Barents Sea: Insights from nitrate isotopes. *Biogeosciences*, *18*(2), 637–653. https://doi.org/10.5194/bg-18-637-2021

Tuerena, R. E., Mahaffey, C., Henley, S. F., de la Vega, C., Norman, L., Brand, T., et al. (2022). Nutrient pathways and their susceptibility to past and future change in the Eurasian Arctic Ocean. *Ambio*, *51*(2), 355–369. https://doi.org/10.1007/s13280-021-01673-0

Tynan, E., Clarke, J. S., Humphreys, M. P., Ribas-Ribas, M., Esposito, M., Rérolle, V. M. C., et al. (2016). Physical and biogeochemical controls on the variability in surface pH and calcium carbonate saturation states in the Atlantic sectors of the Arctic and Southern Oceans. *Deep Sea Research Part II: Topical Studies in Oceanography*, *127*, 7–27. https://doi.org/10.1016/j.dsr2.2016.01.001

Vandieken, V., Nickel, M., & Jørgensen, B. B. (2006). Carbon mineralization in Arctic sediments northeast of Svalbard: Mn(IV) and Fe(III) reduction as principal anaerobic respiratory pathways. *Marine Ecology Progress Series*, *322*, 15–27. https://doi.org/10.3354/meps322015

Wassmann, P., Reigstad, M., Haug, T., Rudels, B., Carroll, M. L., Hop, H., et al. (2006). Food webs and carbon flux in the Barents Sea. *Progress in Oceanography*, *71*(2), 232–287. https://doi.org/10.1016/j.pocean.2006.10.003

Wassmann, P., Slagstad, D., Riser, C. W., & Reigstad, M. (2006). Modelling the ecosystem dynamics of the Barents Sea including the marginal ice zone. *Journal of Marine Systems*, *59*(1), 1–24. https://doi.org/10.1016/j.jmarsys.2005.05.006

Waterson, E. J., & Canuel, E. A. (2008). Sources of sedimentary organic matter in the Mississippi River and adjacent Gulf of Mexico as revealed by lipid biomarker and $\delta^{13}C_{TOC}$ analyses. *Organic Geochemistry*, *39*(4), 422–439. https://doi.org/10.1016/j.orggeochem.2008.01.011

Winkelmann, D., & Knies, J. (2005). Recent distribution and accumulation of organic carbon on the continental margin west off Spitsbergen. *Geochemistry, Geophysics, Geosystems*, *6*(9). https://doi.org/10.1029/2005GC000916

Zaborska, A., Carroll, J., Papucci, C., Torricelli, L., Carroll, M. L., Walkusz-Miotk, J., & Pempkowiak, J. (2008). Recent sediment accumulation rates for the western margin of the Barents Sea. *Carbon Flux and Ecosystem Feedback in the Northern Barents Sea in an Era of Climate Change*, *55*(20), 2352–2360. https://doi.org/10.1016/j.dsr2.2008.05.026

Zeebe, R. E., & Wolf-Gladrow, D. A. (2001). *CO_2 in seawater: Equilibrium, kinetics, isotopes*. Elsevier.
Zhang, C., Dehoff, K., Hess, N., Oostrom, M., Wietsma, T. W., Valocchi, A. J., et al. (2010). Pore-scale study of transverse mixing induced $CaCO_3$ precipitation and permeability reduction in a model subsurface sedimentary system. *Environmental Science & Technology*, *44*(20), 7833–7838. https://doi.org/10.1021/es1019788
Zhang, Y., Yamamoto-Kawai, M., & Williams, W. J. (2020). Two decades of ocean acidification in the surface waters of the Beaufort Gyre, Arctic Ocean: Effects of sea ice melt and retreat from 1997–2016. *Geophysical Research Letters*, *47*(3), e60119. https://doi.org/10.1029/2019GL086421
Zhao, M., Zhang, S., Tarhan, L. G., Reinhard, C. T., & Planavsky, N. (2020). The role of calcium in regulating marine phosphorus burial and atmospheric oxygenation. *Nature Communications*, *11*(1), 2232. https://doi.org/10.1038/s41467-020-15673-3

References From the Supporting Information

Aguilera, D. R., Jourabchi, P., Spiteri, C., & Regnier, P. (2005). A knowledge-based reactive transport approach for the simulation of biogeochemical dynamics in Earth systems. *Geochemistry, Geophysics, Geosystems*, *6*(7), 1–18. https://doi.org/10.1029/2004GC000899
Berner, R. A. (1980). *Early diagenesis: A theoretical approach*. Princeton University Press.
Blouet, J.-P., Arndt, S., Imbert, P., & Regnier, P. (2021). Are seep carbonates quantitative proxies of CH_4 leakage? Modeling the influence of sulfate reduction and anaerobic oxidation of methane on pH and carbonate precipitation. *Chemical Geology*, *577*, 120254. https://doi.org/10.1016/j.chemgeo.2021.120254
Boudreau, B. P. (1997). *Diagenetic Models and Their Implementation: Modelling Transport and Reactions in Aquatic Sediments*. Springer Berlin Heidelberg.
Boudreau, B. P., & Ruddick, B. R. (1991). On a reactive continuum representation of organic matter diagenesis. *American Journal of Science*, *291*(5), 507–538. https://doi.org/10.2475/ajs.291.5.507
Freitas, F. S., Hendry, K. R., Henley, S. F., Faust, J. C., Tessin, A. C., Stevenson, M. A., et al. (2020). Benthic-pelagic coupling in the Barents Sea: An integrated data-model framework. *Philosophical Transactions of the Royal Society A: Mathematical, Physical and Engineering Sciences*, *378*(2181), 20190359. https://doi.org/10.1098/rsta.2019.0359
Jourabchi, P., Van Cappellen, P., & Regnier, P. (2005). Quantitative interpretation of pH distributions in aquatic sediments: A reaction-transport modeling approach. *American Journal of Science*, *305*(9), 919–956. https://doi.org/10.2475/ajs.305.9.919
Regnier, P., Mouchet, A., Wollast, R., & Ronday, F. (1998). A discussion of methods for estimating residual fluxes in strong tidal estuaries. *Continental Shelf Research*, *18*(13), 1543–1571. https://doi.org/10.1016/S0278-4343(98)00071-5
Regnier, P., O'Kane, J. P., Steefel, C. I., & Vanderborght, J. P. (2002). Modeling complex multi-component reactive-transport systems: Towards a simulation environment based on the concept of a Knowledge Base. *Applied Mathematical Modelling*, *26*(9), 913–927. https://doi.org/10.1016/S0307-904X(02)00047-1
Soetaert, K., Hofmann, A. F., Middelburg, J. J., Meysman, F. J. R., & Greenwood, J. (2007). The effect of biogeochemical processes on pH. *Marine Chemistry*, *105*(1–2), 30–51. https://doi.org/10.1016/j.marchem.2006.12.012
Thullner, M., Dale, A. W., & Regnier, P. (2009). Global-scale quantification of mineralization pathways in marine sediments: A reaction-transport modeling approach. *Geochemistry, Geophysics, Geosystems*, *10*(10), 1–24. https://doi.org/10.1029/2009GC002484
Van Cappellen, P., & Wang, Y. (1996). Cycling of iron and manganese in surface sediments; a general theory for the coupled transport and reaction of carbon, oxygen, nitrogen, sulfur, iron, and manganese. *American Journal of Science*, *296*(3), 197–243. https://doi.org/10.2475/ajs.296.3.197
Wehrmann, L. M., Arndt, S., März, C., Ferdelman, T. G., & Brunner, B. (2013). The evolution of early diagenetic signals in Bering Sea subseafloor sediments in response to varying organic carbon deposition over the last 4.3Ma. *Geochimica et Cosmochimica Acta*, *109*, 175–196. https://doi.org/10.1016/j.gca.2013.01.025